Applied Energy 238 (2019) 831–850

Contents lists available at ScienceDirect

Applied Energy

journal homepage: www.elsevier.com/locate/apenergy

Including seismic risk mitigation measures into the Levelized Cost Of Electricity in enhanced geothermal systems for optimal siting

A. Mignan[a,b,c,*], D. Karvounis[b], M. Broccardo[c], S. Wiemer[b], D. Giardini[a]

[a] Swiss Federal Institute of Technology, Zurich, ETHZ, Institute of Geophysics, NO Building, Sonneggstrasse 5, CH-8092 Zurich, Switzerland
[b] Swiss Seismological Service, NO Building, Sonneggstrasse 5, CH-8092 Zurich, Switzerland
[c] Swiss Competence Center for Energy Research-Supply of Electricity, SCCER-SoE, NO Building, Sonneggstrasse 5, CH-8092 Zurich, Switzerland

HIGHLIGHTS

- Seismic risk mitigation cost combined to the heat credit creates a spatial tradeoff.
- The geo-energy pricing increases locally due to induced seismicity risk aversion.
- Safety standards play a central role on spatial optimisation of geo-energy plants.

GRAPHICAL ABSTRACT

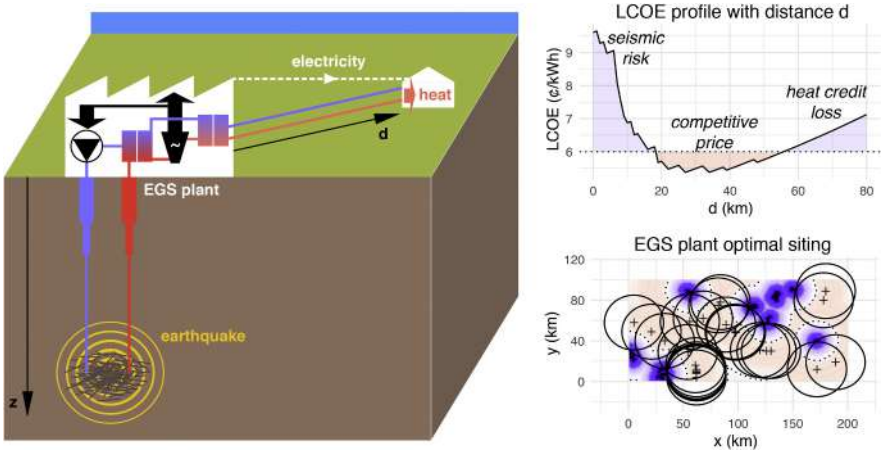

ARTICLE INFO

Keywords:
Levelized Cost Of Electricity
Enhanced geothermal system
Seismicity
Risk mitigation
Meta-model

ABSTRACT

The seismic risk associated with deep fluid injection in Enhanced Geothermal Systems can be mitigated by stopping reservoir stimulation when the seismic risk becomes unacceptable or by reducing production flow rates when seismicity occurs during the operational phase. So far, none of these mitigation measures have been included in the Levelized Cost Of Electricity. A meta-model is introduced that estimates the optimal price of electricity, based on an analytical geothermal energy model, and updates this cost to include the outlay for mandatory seismic risk mitigation measures. The proposed energy model computes both electricity production and heat credit. The costs added during reservoir stimulation are based on the probability of abandoning an injection well, based on a traffic-light system, defined as the ratio of scenarios that exceed a given seismic safety threshold in the risk space. In the production phase, the net energy generated is reduced by clipping the production flow rate so that the reservoir's overpressure does not exceed the regional minimum effective stress. Based on a generic geothermal triplet, we investigate the trade-off between heat credit and seismic risk mitigation cost. The added cost, mostly due to financial risk aversion, shifts the optimal site for a plant from between a few kilometres to tens of kilometres away from populated areas, for increasingly vulnerable building stocks.

* Corresponding author at: Swiss Federal Institute of Technology, Zurich, ETHZ, Institute of Geophysics, NO Building, Sonneggstrasse 5, CH-8092 Zurich, Switzerland.
E-mail address: arnaud.mignan@sed.ethz.ch (A. Mignan).

https://doi.org/10.1016/j.apenergy.2019.01.109
Received 11 June 2018; Received in revised form 21 September 2018; Accepted 17 January 2019

Finally, using a simple yet realistic optimisation strategy, we study the role that a seismic safety standard plays for determining the number of EGS plants that can be sited in a given region.

1. Introduction

Mounting energy needs mean increased interactions with the underground. This can potentially lead to earthquakes, with induced seismicity observed in wastewater disposal from fracking [1], gas extraction [2], CO_2 storage [3], and Enhanced Geothermal Systems (EGSs) [4]. The partial replacement of nuclear energy with geothermal energy [5], or for instance CO_2 sequestration to mitigate climate change [6], transfer various threats to risks of a seismic nature, the impact of which is still poorly understood. With increasing anthropogenic activity, larger, damaging earthquakes have now become a real concern in the United States [1], in the Netherlands [2] and in South Korea [7], raising the question of whether 'tectonic change', similarly to climate change, might be occurring at a regional level.

However, preliminary solutions have been developed to limit induced seismicity, so-called traffic light systems (TLSs) [8]. EGS plants need a TLS during the stimulation phase when earthquakes are deliberately induced to decrease reservoir impedance. The aim during the production phase is to avoid induced seismicity over the plant's lifetime, so lowering the production rate to minimise seismicity is common practice [9]. The former mitigation strategy can lead to the abandonment of an injection well for anything from a short period of time to indefinitely, as was the case for the 2006 Basel EGS project [10], whereas the latter strategy can reduce the plant's net power output, as happened during a recent circulation test at the Soultz EGS reservoir [9]. Both scenarios are expected to push up the price of electricity, due to higher costs and lower energy production respectively. At present, those mitigation strategies are not considered in economic models for EGSs [11], even though induced seismicity is the main risk faced by the industry [10,12].

The aim of the present study is to investigate the increase in EGS's Levelized Cost Of Electricity (LCOE), which is due to the added outlay for seismic risk mitigation measures during both the stimulation and production phases. Since EGSs appear to be indispensable elements in a sustainable, fully renewable energy mix [13], we specifically investigate the trade-off between public seismic safety and geothermal energy's security of supply. The geothermal energy industry needs competitive electricity prices, which are enabled by the sale of EGS direct heat to local populations, but meeting public safety requirements, via a seismic safety standard, increases EGS-related costs close to populated areas. The spatial correlation between heat credit and seismic risk leads to an optimal distance at which the LCOE is minimal, which we will consider with a view to optimising the siting of EGS plants to the extent permitted by safety standards.

This paper is structured as follows: Section 2 presents the background research available on EGS energy economics and induced seismicity risk mitigation. Section 3 introduces a meta-model comprising an energy model that computes both electricity generation and heat production, an economic model, a seismic risk model, and a behavioural decision-making model. Section 4.1 shows a synthetic case study in which the siting of a generic EGS triplet is optimised by minimising the LCOE as a function of the plant's energetic profile, exposure building class, stakeholder behaviour, and the safety standard threshold. Section 4.2 presents synthetic exposure maps where the number of EGS plants to be sited is optimised in order to illustrate how different safety standards impact the potential EGS electricity supply. Finally, Section 5 provides the conclusions of our work and directions for future improvements.

2. Background

2.1. EGS energy economics

Global climate change mitigation measures and the planned phasing out of nuclear energy in some countries mean that new energy sources are needed. So far, renewable energy represents the best option. Since solar and wind energy are inherently intermittent [13], smart grids are being developed to optimise the power grid, so that a round-the-clock base load is still attained. Existing methods are based on optimal control theory [14], artificial intelligence [15], and – since very recently – blockchain technology [16,17].

One strategic source of renewable energy is deep geothermal energy, a resource that can provide up to 8.3% of total world electricity production [18] since it can be developed virtually anywhere. For its utilisation to approach this upper limit, the further development of EGS and of non-conventional geothermal technologies is necessary. These technologies aim to competitively extract the stored heat by stimulating deep geothermal reservoirs and by artificially creating a network of highly permeable fractures with optimal spacing (Fig. 1). Lu [19] provides the most up-to-date review of EGS literature, covering technological and economic aspects, life cycle and environmental assessments and describing models as well as existing EGS plants. Apart from being readily available, the base-load nature of an EGS power plant, independent of weather conditions and seasonal effects, makes it a crucial complement to a secure renewable energy mix [13]. EGS's ubiquity and stability explain its importance in national energy roadmaps. Examples include the 2006 report entitled “The Future of Geothermal Energy” [20], summarised by Tester et al. [21], and the 2015 report entitled “Energy from the Earth, Deep Geothermal as a Resource for the Future?” by the Swiss Centre for Technology Assessment (TA Swiss) [22].

Although EGS's LCOE remains relatively high, technological advancements, especially in drilling, are expected to substantially lower it over the next few decades [23]. The LCOE can already be reduced through heat credit, whereby waste heat is sold to nearby consumers for direct heating, as a complement to generated electricity [24]. Since

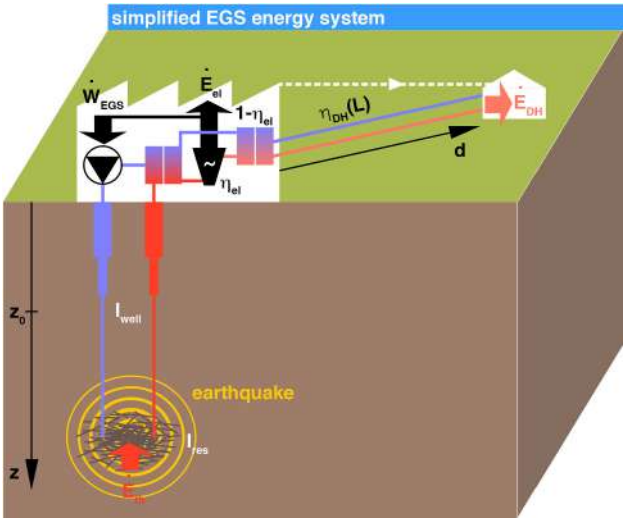

Fig. 1. Simplified EGS energy system consisting of three cycles: an EGS cycle, a conversion cycle, and a district heating cycle (see Table 1 for parameter definitions).

heat is steadily lost as it is transmitted further away from the plant, taking advantage of the heat credit requires EGS plants to be sited close to populated areas. The 2006 Basel EGS project was sited within Basel, Switzerland, exactly to maximise such a benefit [25]. However, this also meant induced seismicity had a higher impact on the populations, and it was this that ultimately prompted the project's termination after a moderately sized earthquake caused non-structural damage [10].

The trade-off between heat credit value and seismic risk level remains to be fully quantified. An environmental analysis of EGS practical design options by Lacirignola and Blanc [12] showed that the risk of induced seismicity is a key discriminating factor, as it increases proportionally to the environmental benefit. Knoblauch and Trutnevyte [26] made a first semi-quantitative analysis of the trade-off between heat benefits and induced seismicity risks, verifying that a medium- to large-size EGS near some medium-size population would be most beneficial. Olasolo et al. [11] emphasised economic models' failure so far to take account of the seismic factor. Bartlett et al. [13] suggested that 28 plants, generating an average output each of 18 MW, would be needed for a fully renewable Swiss energy grid. Jain et al. [27] showed that 13,450 EGS plants could theoretically be created in Germany, though this scenario should be seen as a very optimistic thought experiment maximising the potential of geothermal power. The feasibility of such geothermal energy scenarios will always depend on the level of acceptable seismic risk in a given jurisdiction.

2.2. Induced seismicity risk mitigation strategies and pricing

Induced seismicity has delayed or cancelled several recent EGS projects, proving that “geothermal quake risks must be faced” [10]. Majer et al. [4] reviewed cases of EGS-related induced seismicity and their possible causes, and concluded that if site selection is carried out properly there is no need for seismic risks to pose a threat to the development of the geothermal energy industry.

Induced seismicity can be mitigated during an EGS project by using a TLS, which boosts public safety but may affect a new plant's economic viability. A TLS is based on a decision variable (earthquake magnitude, peak ground velocity, *etc.*) and a threshold above which actions (e.g. stopping the injection or reducing production rates) must be taken. An early example of TLS deployment at an EGS site, in El Salvador in 2003, is described by Bommer et al. [8]. It was a TLS that terminated the 2006 Basel project [25], due to the plant's proximity to populated areas [28]. The definition of the TLS threshold is currently based on expert judgment, regulations, and simple heuristics [29].

Probabilistic seismic risk assessment is now advocated for the management of induced seismicity. Mignan et al. [28] applied such a method to the 2006 Basel experiment, considering the impact of epistemic uncertainties in a logic tree approach. Baker and Gupta [30] reviewed traditional probabilistic seismic hazard analysis and presented a Bayesian approach for updating results when new information becomes available during reservoir stimulation. A hierarchical Bayesian framework was proposed by Broccardo et al. [31] for updating induced seismicity data online.

Mignan et al. [32] recently proposed an actuarial approach to induced seismicity risk mitigation, where the TLS verifies a specific risk-based safety standard. Considering the norms and standards already in use in other hazardous industries [33] finally enabled the financial costs of implementing a TLS to be quantified. In view of the central role of induced seismicity risk in the EGS industry, Mignan et al. [34] integrated the cost of TLS measures, in terms of injection well loss, into the LCOE and showed that it increases closest to populated areas. However, they did not investigate the spatial trade-off with heat credit.

Table 1
Metamodel parameterization.

Parameter	Value range[a]	Refs./ Comments
EGS cycle, conversion cycle		
z [m]	[4000; 9000]	N/A
dT/dz [°C/ km]	[30; 40]	[22]
T_0 [°C]	15	N/A
T_{inj} [°C]	[60; 75]	[22]
c_w [J/(kg K)]	4180	N/A
g [m/s^2]	9.81	N/A
ρ [kg/m^3]	$1030–0.1625T–0.00269T^2$	T in °C
ρ_{rock} [kg/m^3]	2500	Similar to granite
η_{el} [ ]	$0.078795\ln(c \cdot dT/dz + h_{inj}) - 1.00081$	[35]
N_{res}, N_{inj}, N_{prod} [ ]	Doublet: 1, 1, 1 Triplet: 2, 2, 1 3-stage doublet: 3, 1, 1	N/A
a_{inj} [ ]	2	N/A
I_{res} [Pa s/m^3]	$2 \cdot 10^8$	[22]
I_{w0} [Pa s/m^3]	$3.3 \cdot 10^8$	Basel case
D_w [m]	0.25	Basel case
z_0 [m]	2500	Basel case
μ [Pa s]	$243.18 \cdot 10^{-7} \cdot 10^{247.8/(T+273-140)}$	[69], T in °C
ν [ ]	0.25	N/A
σ_S [ ]	10%	[50]
District heating cycle		
U [W/(K m)]	8	N/A
L [km]	[0; 50]	N/A
T_s [°C]	50	N/A
Costs		
Δt_{EGS} [yr]	[20; 30]	[22]
$n_{hr,el}$ [hr/yr]	8000	N/A
$n_{hr,DH}$ [hr/yr]	2500	[22]
Δt_{well} [yr]	[5; 30]	[22]
r_{renew} [ ]	$\text{round}[(\Delta t_{plant} - \Delta t_{well})/\Delta t_{well}]$	N/A
$\min(C_{well})$ [$]	$(1.72 \times 10^{-7}z^2 + 2.3 \times 10^{-3}z - 0.62) \times 10^6$	[37]
C_{well} [$]	$[\min(C_{well}); 2 \cdot \min(C_{well})]$	N/A
C_{frac} [$]	10^6	[22]
$\min(C_{plant})$ [$]	$\{750 + 1125 \exp[-0.006115\ (10^{-6}\ P_{net} - 5)]$ $10^{-3}\ P_{net}\}$	[20]
C_{plant} [$]	$[\min(C_{plant}); 2 \cdot \min(C_{plant})]$	N/A
C_1 [€/m]; C_2 [€/m^2]	151; 1378	[38]
D_{DH} [m]	0.5	[38]
r_{market} [ ]	1/3	N/A

[a] Parameter distributions considered random uniform within those ranges.

3. Enhanced geothermal system meta-model

3.1. Energy production model

The simplified energy system considered here consists of three cycles: an EGS cycle, a conversion cycle, and a district heating cycle (Fig. 1). The EGS is responsible for upstreaming the geothermal heat to the surface, while the conversion and district heating cycles are responsible for downstreaming electrical and heating power to consumers, respectively. In the analysis that follows, S.I. units should be considered when a unit has not been explicitly specified. The list of input parameters is given in Table 1.

The EGS cycle consists of the wells, the geothermal reservoir, a geothermal pump and a heat exchanger with the conversion cycle. A cold fluid of enthalpy h_{inj} is always re-injected through the well while a fluid of elevated enthalpy h_{prod} is produced in the reservoir. The upstreamed geothermal heat $\dot{E}_{th}$ is considered steady in time but increases with depth z at a constant rate, such that

$$\dot{E}_{th}(z) = \rho_{inj}\dot{V}_{inj}(h_{prod} - h_{inj}) = \rho_{inj}\dot{V}_{inj}c_w\left(T_0 + z\frac{dT}{dz} - T_{inj}\right) = \rho_{inj}\dot{V}_{inj}c_w\Delta T \quad (1)$$

where $\dot{V}_{inj}$ is the injected flow rate, ρ_{inj} the fluid density at injection temperature T_{inj}, c_w the specific heat capacity of water (considered constant), T_0 the temperature at zero depth, and dT/dz the geothermal gradient.

$\dot{E}_{th}$ is then converted into market electrical power $\dot{E}_{el}$ by expanding vapour in the conversion cycle, subject to efficiency η_{el} [35] and minus the converted electrical power $\dot{W}_{EGS}$ that feeds the EGS pump, as

$$\dot{E}_{el} = \eta_{el}\dot{E}_{th} - \dot{W}_{EGS} \quad (2)$$

The converted electrical power $\dot{W}_{EGS}$ compensates for pressure losses inside the reservoir and wells, ΔP_{res} and ΔP_{well}, respectively, minus the pressure gains ΔP_g due to gravitational effects, as

$$\dot{W}_{EGS} = (\Delta P_{res} + \Delta P_{well} - \Delta P_g)\dot{V}_{inj} \quad (3)$$

with

$$\begin{cases} \Delta P_{res} = \frac{I_{res}}{N_{res}}\dot{V}_{inj} \\ \Delta P_{well} = I_{well}\dot{V}_{inj}^{1.75} \\ \Delta P_g = \rho g(\rho_{inj} - \rho_{prod}) \end{cases} \quad (4)$$

where I_{res} is the reservoir impedance, I_{well} is the wells' impedance for a turbulent flow [Pa(s/m^3)$^{1.75}$], N_{res} is the number of independent and identical flow paths (N_{res} = 1 for doublets, 2 for triplets when an interconnected network of flow paths is assumed), and g is the gravitational acceleration (see Appendix A for a demonstration of ΔP_{well} and definition of I_{well}).

In a realistic setting, $\dot{V}_{inj}$ would be optimised to reach the maximum electrical power $\dot{E}_{el}$. The simplified energy system considered here yields the following non-linear equation

$$\dot{E}_{el} = -I_{well}\dot{V}_{inj}^{2.75} - \frac{I_{res}}{N_{res}}\dot{V}_{inj}^2 + [\eta_{el}\rho_{inj}c_w\Delta T + \rho g(\rho_{inj} - \rho_{prod})]\dot{V}_{inj} \quad (5)$$

Being of the form $\dot{E}_{el} = a\dot{V}_{inj}^{2.75} + b\dot{V}_{inj}^2 + c\dot{V}_{inj}$, there is an optimum $\dot{V}_{opt}$ that maximises electrical revenue and satisfies

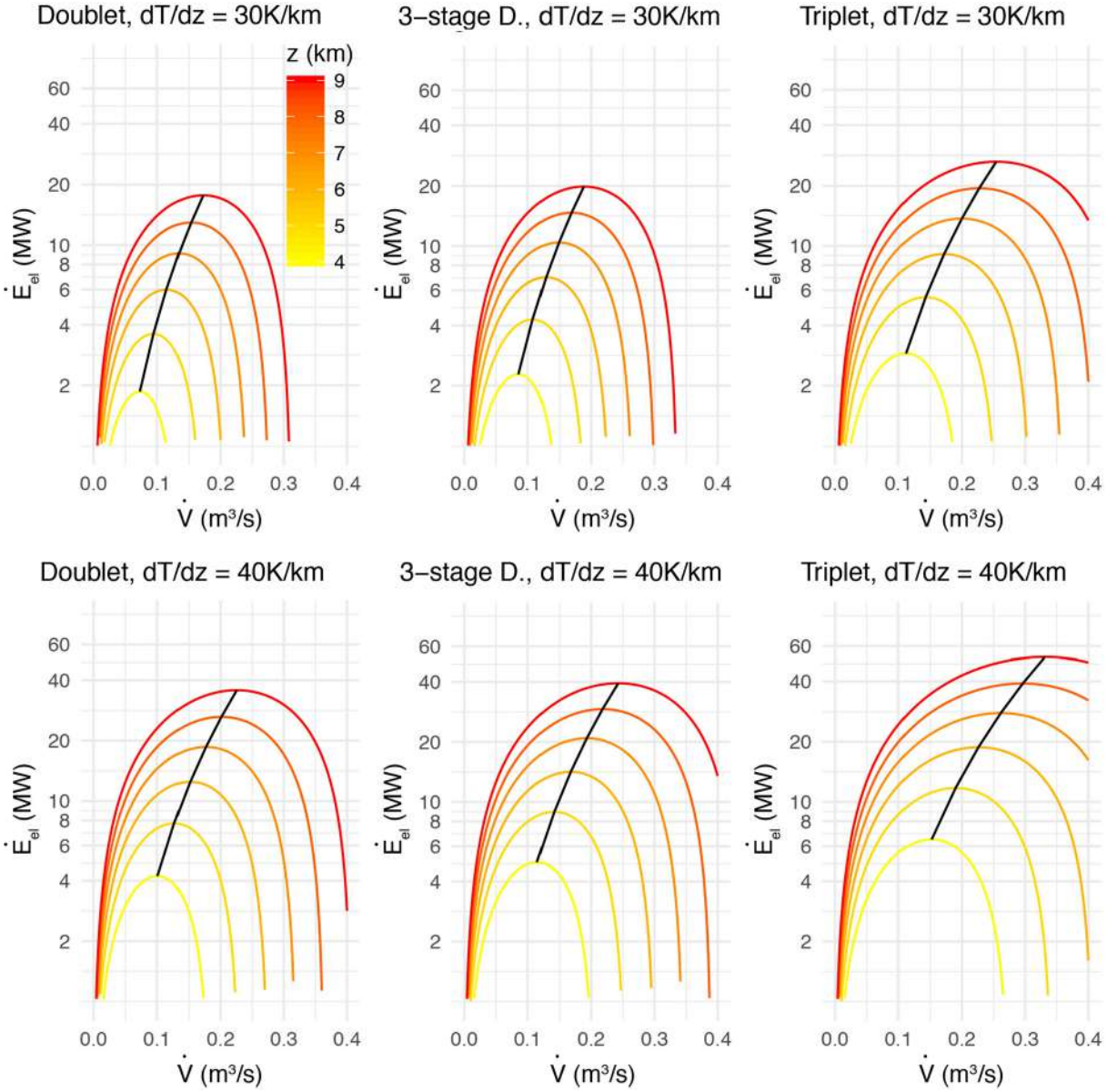

Fig. 2. Relationship between injected flow rate $\dot{V}$ and electric power produced $\dot{E}_{el}$, with the optimal flow rate $\dot{V}_{opt}$ represented by the black curves.

$$\frac{d\dot{E}_{el}}{d\dot{V}}(\dot{V}_{opt}) = 2.75a\dot{V}_{opt}^{1.75} + 2b\dot{V}_{opt} + c = 0 \quad (6)$$

This can be easily solved numerically, or by the following approximation

$$\dot{V}_{opt} \approx \frac{-B_1 \pm \sqrt{B_1^2 - 4A_1C_1}}{2A_1} + \frac{-2b \pm \sqrt{4b^2 - 2.75a}}{1.375a} \quad (7)$$

where only the positive value of each term is meaningful. See Appendix B for the definition of A_1, B_1, C_1 and the demonstration of Eq. (7) as the approximated solution to Eq. (6) for the $\dot{V}$ range considered. Fig. 2 plots different parameterisations of Eq. (5), i.e., different values of z, gradient dT/dz, and EGS plant type N_{res}, as well as the optimal flow rate defined in Eq. (7), which is verified to give reasonable estimates of $\max(\dot{E}_{el})$. Henceforth, only EGS triplets are considered.

The nominal flow rate $\dot{V}_{nom} = \dot{V}_{opt}$ is considered for the baseline LCOE calculation of Section 3.2. However, this represents the most optimistic option, as a high production flow rate may lead to unwanted induced seismicity during the EGS plant's operational phase [9]. To minimise seismicity, the reservoir overpressure ΔP_{res} should not exceed the minimum effective stress $S_{hmin} - P_h = \nu/(1-\nu)\cdot(S_V - P_h)$, where S_{hmin} is the minimum stress, $P_h = \rho_{inj}gz$ the hydrostatic pressure, $S_V = \rho_{rock}gz$ the vertical stress, and ν Poisson's ratio [36]. Fig. 3a represents the stress depth profile including a Gaussian noise for different standard deviations σ_S. We then define the clipped production flow rate as

$$\dot{V}_{cap} = \begin{cases} \frac{S_{min}(1-3\sigma_S) - P_h}{I_{res}}, & \text{if } \dot{V}_{opt}I_{res} + P_h > S_{min}(1-3\sigma_S) \\ \dot{V}_{opt}, & \text{otherwise} \end{cases} \quad (8)$$

which means that we expect no seismicity with $3\sigma_S$ confidence. Fig. 3b shows the dramatic impact of σ_S on $\dot{V}_{cap}$. The impact on the LCOE of seismicity mitigation during the production phase is thus obtained by setting the nominal flow rate $\dot{V}_{nom}$ to $\dot{V}_{cap}$ instead of $\dot{V}_{opt}$. This will be investigated in the case study of Section 4.

The heat exchanger of the district heating cycle absorbs the waste heat of the conversion cycle and downstreams to an existing urban district heating facility the following heat:

$$\dot{E}_{DH} = (1-\eta_{el})\eta_{DH}\dot{E}_{th} = \eta_{DH}\dot{E}_{DH,0} \quad (9)$$

where η_{DH} is the portion of thermal heat that reaches the destination and $\dot{E}_{DH,0}$ is the waste heat leaving the conversion cycle (Fig. 4a). Note that the pumping losses are neglected. An exponential decline is assumed for heat losses along the supply pipe by

$$\eta_{DH} = \exp\left(-\frac{UL}{\rho_{DH}\dot{V}_{DH}c_w}\right) \quad (10)$$

where U is the insulation value, $\dot{V}_{DH}$ is the flow rate of water along the pipe (not to be confused with $\dot{V}_{nom}$) and L is the distance from the plant along the supply pipe (Fig. 4b). Here, heat losses along the return pipe are neglected. Eq. (10) is consistent with the solution of the one-dimensional steady advection-convection for a cylinder with a constant wall temperature.

The nominal flow rate $\dot{V}_{DH,nom}$ must satisfy the condition

$$\rho_{DH}\dot{V}_{DH,nom}c_w\Delta T_s = \eta_{DH}\dot{E}_{DH,0} \Leftrightarrow \frac{\rho_{DH}c_w\Delta T_s}{\dot{E}_{DH,0}} = \frac{1}{\dot{V}_{DH,nom}}e^{\left(-\frac{UL}{\rho_{DH}c_w}\frac{1}{\dot{V}_{DH,nom}}\right)} \quad (11)$$

to minimise heat losses and where $\Delta T_s = T_s - T_0$ is the supply temperature gradient (i.e., the difference between supply temperature T_s and ground temperature T_0). The solution to Eq. (11) is

$$\dot{V}_{DH,nom} = -\frac{UL}{\rho_{DH}c_w W_0\left(-\frac{UL\Delta T_s}{\dot{E}_{DH,0}}\right)} \quad (12)$$

where W is the Lambert function (i.e., $x = W(y) \Rightarrow y = xe^x$). Here we consider the main branch W_0 so that $\dot{V}_{DH,nom} \to +\infty$ when $\Delta T_s \to 0^+$. Substituting $\dot{V}_{DH,nom}$ for its value in Eq. (10), it follows that the maximum (and also nominal) proportion of waste heat from the conversion cycle that can be commercially exploited for heating is

$$\eta_{dh,nom} = \begin{cases} 0, & \text{if } \dot{E}_{dh,0} < eUL\Delta T_s \text{ or } \dot{V}_{dh,nom} < \dot{V}_{nom} \\ \exp\left[W_0\left(-\frac{UL\Delta T_{min}}{\dot{E}_{DH,0}}\right)\right], & \text{otherwise} \end{cases} \quad (13)$$

where e is Euler's constant (Fig. 3b). Around 0, W_0 is asymptotic to $W_0(y) = y - y^2 + 3/2\ y^3 - 8/3\ y^4 + 125/24\ y^5 - \ldots$ with $y = -UL\Delta T_{min}/[(1-\eta_{el})\dot{E}_{th}]$ in our case. The role of depth z (via η_{el}) and supply pipe length L (via η_{DH}) on district heat energy $\dot{E}_{DH}$ is shown in Fig. 4c. District heat power $\dot{E}_{DH}$ then leads to the heat credit part of the LCOE, as described below in Section 3.2. Its dependence on distance from the EGS plant is at the origin of the trade-off with seismic risk, which also depends on the distance to the populations, as modelled in Section 3.3.

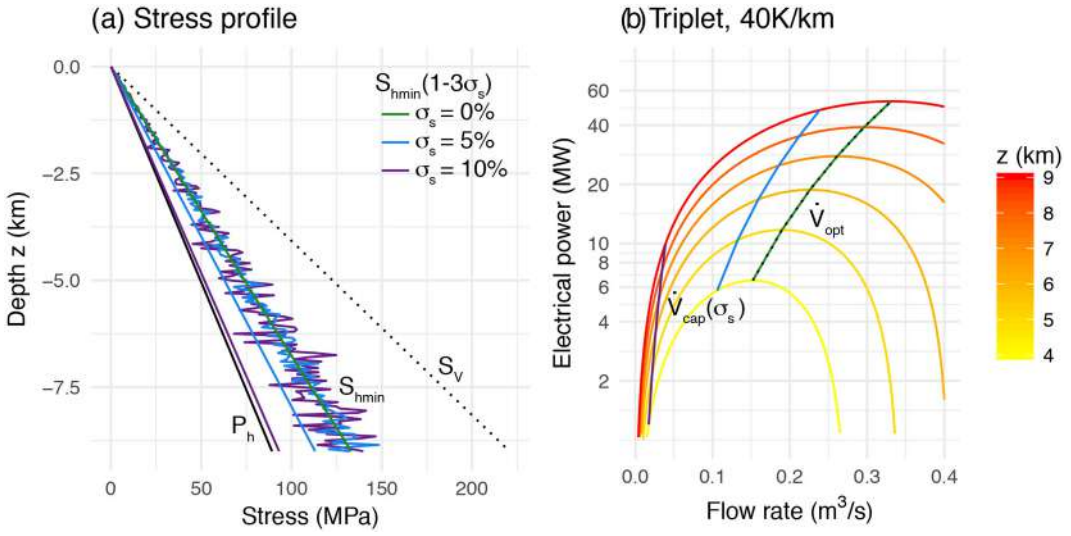

Fig. 3. Flow rate clipping for induced seismicity minimisation during the production phase.

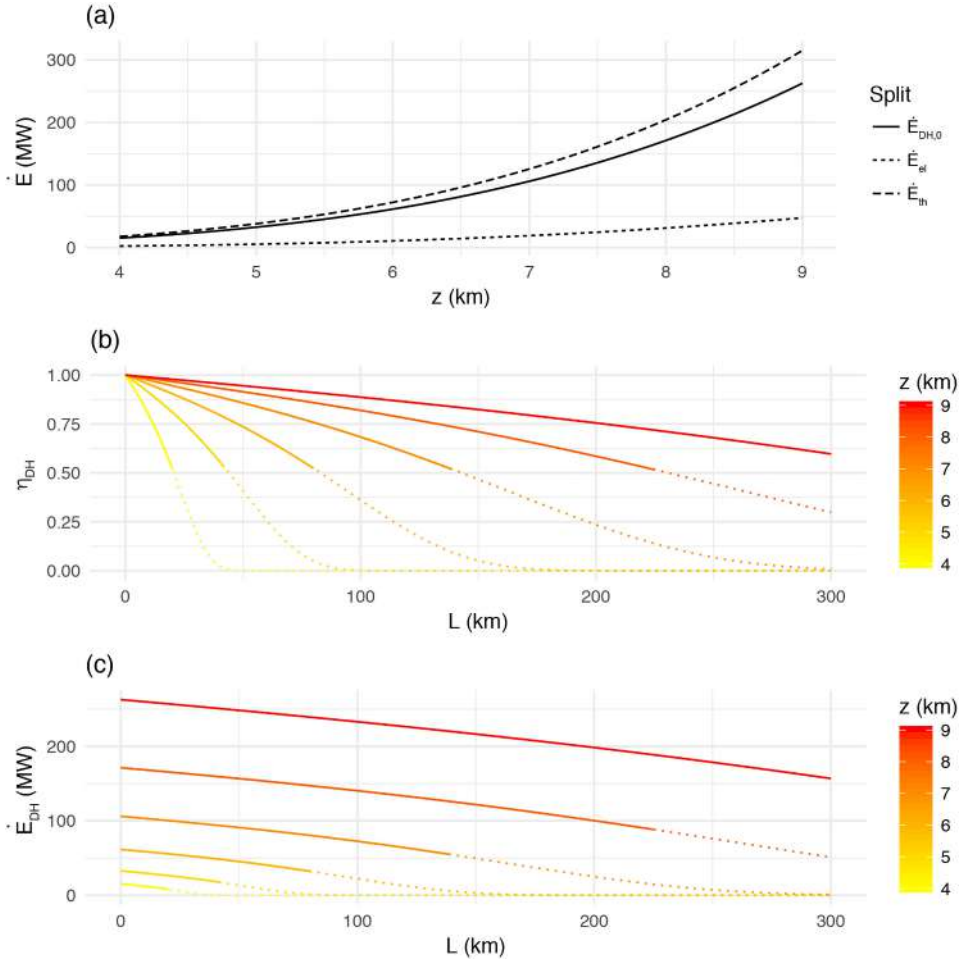

Fig. 4. District heating model results for an EGS triplet and thermal gradient $dT/dz = 40\,^{\circ}\mathrm{C}$.

3.2. Economic model

The LCOE is the total cost C to build and operate an EGS plant, divided by the total energy E produced over the plant lifetime, which we formulate in terms of price $P_{EGS} = C_{EGS}/E_{EGS}$. We first get $E_{EGS}(z) = n_{hr,el}\Delta t_{EGS}\dot{E}_{el}(z)$ with $\dot{E}_{el}$ from Section 3.1, $n_{hr,el}$ the number of operating hours per year (for electricity), and Δt_{EGS} the plant lifetime in years. The cost is estimated from

$$C_{EGS}(z) = n_{well}(C_{well}(z) + C_{frac}) + C_{plant}(\dot{E}_{el}(z)) + r_{renew}n_{well}C_{well}(z) \tag{14}$$

where n_{well} is the number of wells, C_{well} is the cost of well drilling [37], C_{frac} is the cost of fracturing per well, C_{plant} is the cost of the EGS plant [20], and r_{renew} is the rate of well renewal during the plant lifetime (Table 1). For heat, we consider the cost of pipeline construction

$$C_{DH}(L) = (C_1 + C_2 D_{DH})L \tag{15}$$

as a function of pipeline length L between the power plant and the existing heat district, where C_1 is the construction cost constant, C_2 is the construction cost coefficient and D_{DH} is the mean pipe diameter [38]. Similarly to electricity, we get the district heating energy $E_{DH} = n_{hr,DH}\Delta t_{EGS}\dot{E}_{DH}$ with $\dot{E}_{DH}$ from Section 3.1 and $n_{hr,DH}$ the number of operating hours per year for heat.

We then define the EGS LCOE with heat credit as

$$P_{EGS+DH}(z, L) = \frac{E}{C} = \frac{E_{EGS}(z) + r_{market}E_{DH}(z, L)}{C_{EGS}(z) + C_{DH}(L)} \tag{16}$$

where r_{market} corrects for the market price of heating being lower than that of electricity. We simulate 10,000 scenarios sampling input parameters from uniform random distributions bounded by the ranges given in Table 1. The results are represented by the median curve, 25–75% ribbon and 5–95% ribbon in Fig. 5 for the net electrical power $\dot{E}_{el}$, the drilling costs C_{well}, the total EGS costs C_{EGS}, and finally the estimated LCOE both without heat credit, P_{EGS} (in orange), and with maximum heat credit, P_{EGS+DH} (in red, for $L = 0$ km).

The proposed economic model is benchmarked against the U.S. Department of Energy's Geothermal Electricity Technologies Evaluation Model, or GETEM [21], the GEOPHIRES software tool [24] which is an upgrade from the MIT-EGS program [20,21], the Swiss Centre for Technology Assessment model TA Swiss [22] and the work by Lacirignola and Blanc [12]. In general, more detailed and complex models should be used that include various technologies, such as energy conversion and drilling [39], as well as a full life cycle analysis [40]. Here, our parameter range is mainly constrained to the TA Swiss analysis, though we do not consider thermal drawdown nor interest rate. Both the GETEM and CH-estimates shown in Fig. 5 are from the TA Swiss study [22]. Asterisks indicate that the TA Swiss values were re-estimated using Eq. (14) for total EGS costs. The downward arrow represents the 7 ¢/kWh heat credit given by TA Swiss. L&B13 refers to

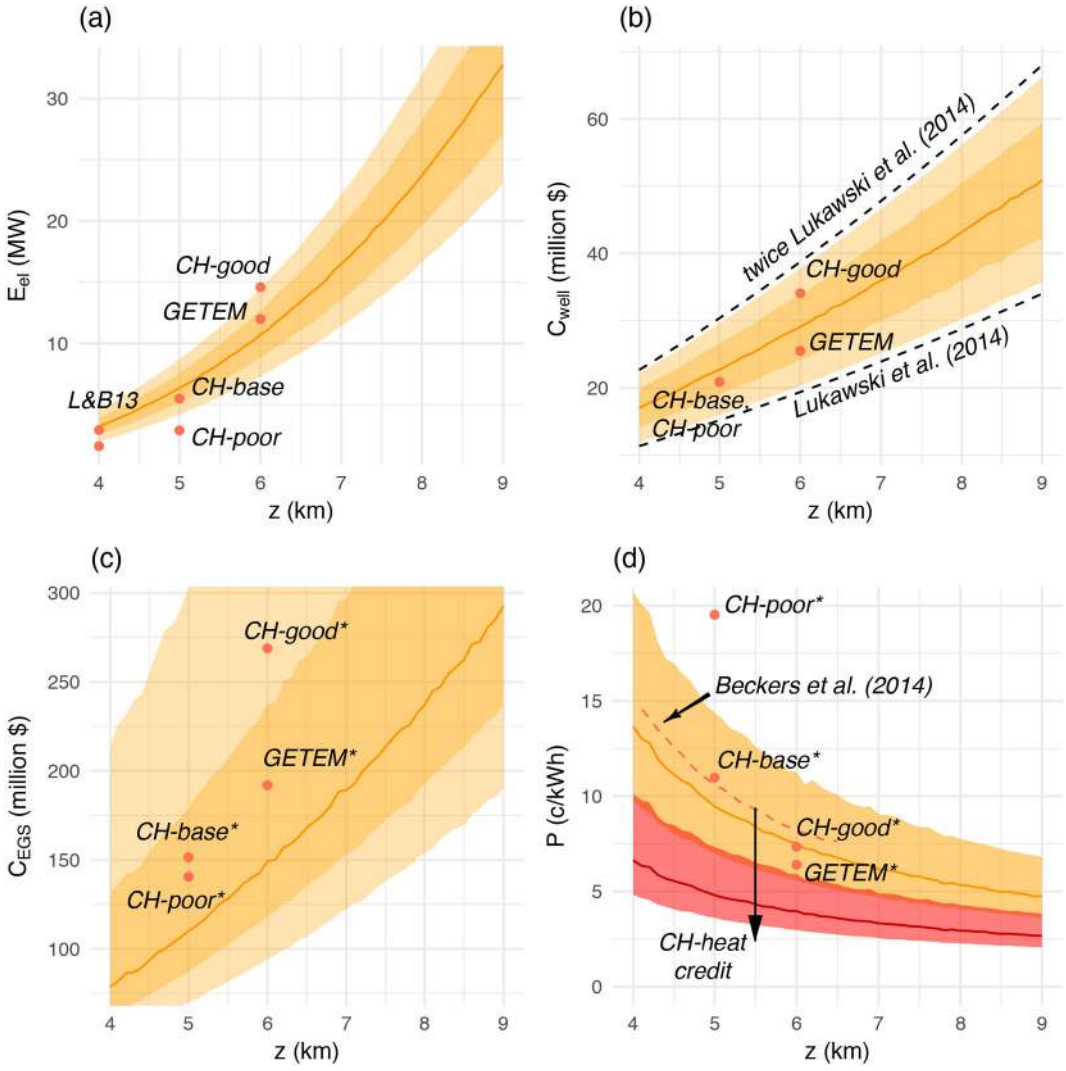

Fig. 5. Economic model parameters and pricing P as a function of borehole depth z.

cases 5–6 of Lacirignola and Blanc. We assumed an exchange rate of USD 1 = CHF 1 = EUR 0.8. Comparison with GEOPHIRES suggests that our results are mildly optimistic compared to the actual EGS technology since we obtain similar prices to GEOPHIRES, but for lower temperature gradients. Nonetheless the general LCOE level and dependence on depth is retrieved, as is the maximum heat credit. While we use these numbers as our base case in the rest of our study, other LCOE models could be used without significantly altering our conclusions.

3.3. Induced seismicity risk model

We postulate that moving from EGS feasibility test sites to operational EGS plants will require the implementation of quantitative seismic safety norms. Since there is still no standard risk-based regulation in place for EGS (for magnitude-based regulations, see [29]), we define a safety standard consistent with other hazardous industries [33,41], namely the individual risk IR, i.e., the probability of a statistically representative individual dying within a given timeframe and at a given location. Mignan et al. [32] showed how an autonomous TLS would stop the reservoir stimulation so that a given IR threshold is respected on average. In that context, we can estimate the probability p of a TLS stopping reservoir stimulation because of an unacceptable seismic risk [34]. The method entails first assessing the induced seismicity hazard, then the risk, and finally ascertaining whether the safety standard is or is not respected in different risk scenarios. The induced seismic hazard is assessed as the probability of exceeding a given intensity at a given distance d from the EGS plant, based on the number of events N during the stimulation, the maximum possible magnitude M_{max}, and an empirical intensity prediction equation.

The rate of seismicity λ induced during reservoir stimulation can be described by

$$\lambda(t, \geq m) = 10^{a-bm}\dot{V}_{stim}(t) \tag{17}$$

where $\dot{V}_{stim}(t)$ is the injected flow rate [m^3/day] at time t (not to be confused with the production flow rate of Section 3.1), m is the earthquake magnitude, a is the seismic activation and b is the earthquake magnitude ratio. Eq. (17) is valid for a number of deep underground stimulations [32] and can be explained by both poroelasticity [42] and static stress overpressure [43]. Integrating Eq. (17) yields the number of earthquakes $N(\geq m) = 10^{a-bm}V$ as a function of the total fluid volume V [m^3] injected during stimulation. We estimate N from (a, b) values observed in 13 stimulations, with $-4.2 \leq a \leq 0.1$ and

Table 2
Underground seismic feedback to deep fluid injection.

Site (country*, year)	$a^{\dagger}$ [m^{-3}]	b	Ref.
Ogachi (JP, 1991)	−2.6	0.7	[42]
Ogachi (JP, 1993)	−3.2	0.8	[42]
Soultz (FR, 1993)	−2.0	1.4	[42]
KTB (DE, 1994)	−1.4	0.9	[32]
Paradox Valley (US, 1994)	−2.4	1.1	[32]
Soultz (FR, 1995)	−3.8	2.2	[42]
Soultz (FR, 1996)	−3.1	1.8	[42]
Soultz (FR, 2000)	−0.5	1.1	[42]
Cooper Basin (AU, 2003)	−0.9	0.8	[42]
Basel (CH, 2006)	0.1	1.6	[32]
KTB (DE, 2004–5)	−4.2	1.1	[42]
Newberry (US, 2012)	−2.8	0.8	[32]
Newberry (US, 2014)	−1.6	1.0	[32]

* ISO code.
† Referred to as seismogenic index in Dinske and Shapiro (2013).

$0.7 \leq b \leq 2.2$ (Table 2; Fig. 6a) and a fixed total injected volume V of 30,000 m^3 to reach an operational reservoir size. This represents an average value taken from a realistic range of 5000–50,000 m^3 [44]. We do not investigate the role of different V values since the impact on N would be equivalent to changing the a-value of only one unit.

Although M_{max} has long been constrained by V [45,46], van der Elst et al. [47] demonstrated that induced seismicity observations tally with a tectonic M_{max} null-hypothesis. Note in this connection that the recent 2017 Pohang earthquake is a clear violation of the McGarr limit (Fig. 6b) [48]. This does not mean that the McGarr method is invalid, merely that it cannot consider the possible triggering of pre-loaded faults, which is at the basis of the on-going debate on induced versus triggered seismicity and the lack of expert consensus on M_{max} [49]. As a consequence, we test both theories with

$$\begin{cases} M_{max,McGarr}(V) = \frac{2}{3}\log_{10}(GV) - 10.7 + \frac{14}{3} \\ M_{max,tect} = 7 \end{cases} \quad (18)$$

where the maximum seismic moment is $M_{0max} = GV$ [N m] and $G = 3.10^{10}$ Pa is the modulus of rigidity [45]. Although some physical models also predict an increase of M_{max} with borehole depth [50], more evidence is still needed before implementing them in seismic risk analyses. To move from magnitude to hazard, we test four regional intensity attenuation relationships representative of California, Central and Eastern U.S. [51], Switzerland [52] and a global dataset [53], truncating hazard at 3σ. The four empirical relationships are listed in Table 3 and shown in Fig. 6c.

Risk of damage is then assessed using the RISK-UE macroseismic approach [28] from which we estimate the mean damage grade

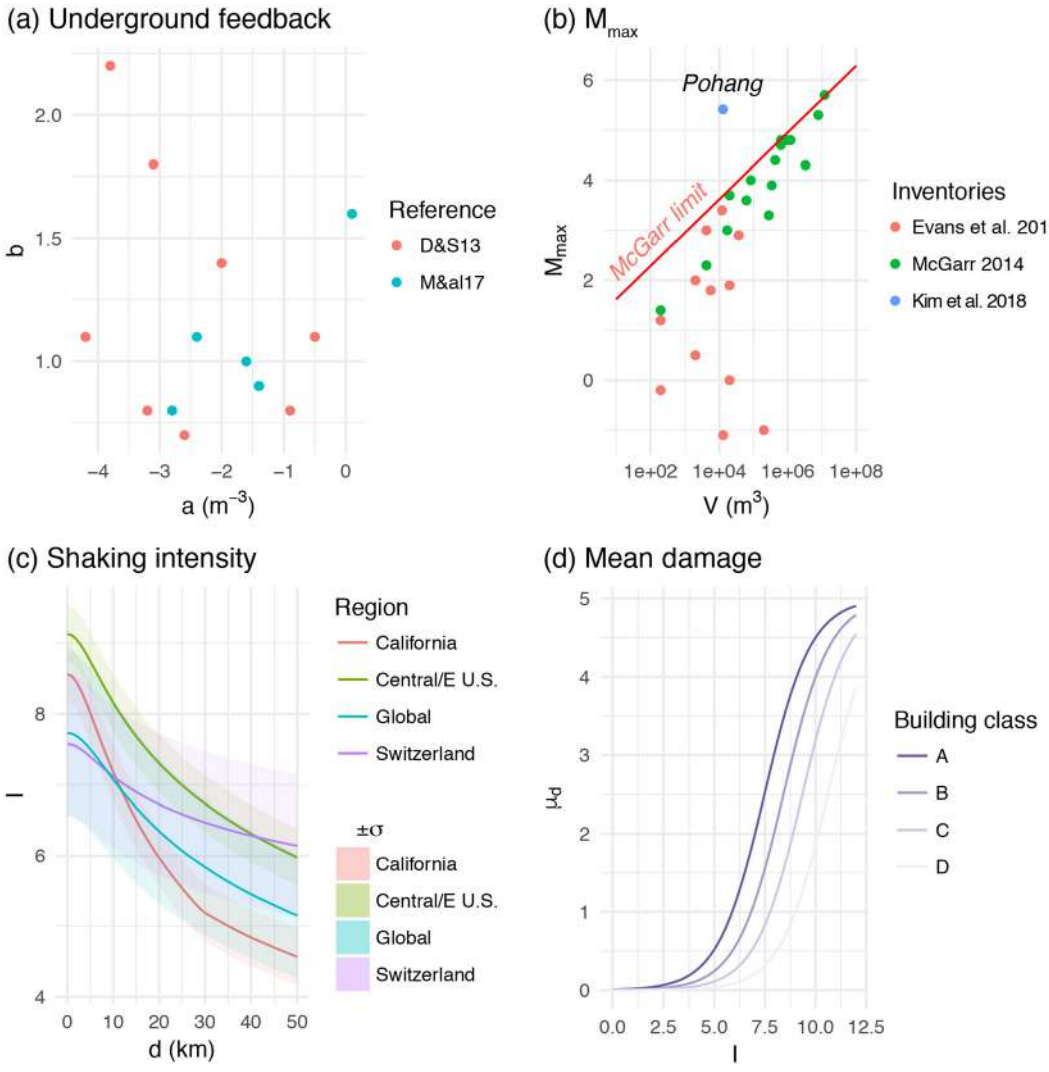

Fig. 6. Inputs of the induced seismicity risk analysis.

Table 3
Empirical magnitude-intensity relationships for seismic hazard assessment.

Region	Relationship	Parameters	Reference
California	$I = c_1 + c_2(m-6) + c_3(m-6)^2 + c_4\log_{10}d_h + c_5 d_h + c_6 B + c_7 m\log_{10}d_h$	$c_1 = 12.27$, $c_2 = 2.270$, $c_3 = 0.1304$, $c_4 = -1.30$, $c_5 = -0.0007070$, $c_6 = 1.95$, $c_7 = -0.577$, $R_t = 30$ km, $\sigma = 0.4$	[51]
Central/Eastern U.S.A		$c_1 = 11.72$, $c_2 = 2.36$, $c_3 = 0.1155$, $c_4 = -0.44$, $c_5 = -0.002044$, $c_6 = 2.31$, $c_7 = -0.479$, $R_t = 80$ km, $\sigma = 0.4$	
Switzerland	$I = \frac{m - c_2\log\left(\frac{d_h}{30}\right) - c_3(d_h - 30) - c_0}{c_1}$	$c_0 = 1.2567$, $c_1 = 0.7317$, $c_2 = 0.5062047$, $c_3 = -0.000614628$, $\sigma = 1$	[52]
Global	$\begin{cases} I = c_0 + c_1 m + c_2\log\sqrt{d_h^2 + (c_3 + c_4\exp(m-5))^2} \\ \sigma = s_1 + \frac{s_2}{1 + \left(\frac{d_h}{s_3}\right)^2} \end{cases}$	$c_0 = 2.085$, $c_1 = 1.428$, $c_2 = -1.402$, $c_3 = -0.209$, $c_4 = 2.042$, $s_1 = 0.82$, $s_2 = 0.37$, $s_3 = 22.9$	[53]

$$\mu_D = 2.5\left[1 + \tanh\left(\frac{I + 6.25V_i - 13.1}{Q_d}\right)\right] \tag{19}$$

where $0 < \mu_D < 5$, $Q_d = 2.3$ is the ductility index, and V_i is the vulnerability index [54], a proxy to the EMS-98 building classification [55]. Eq. (19) is represented in Fig. 6d for $V_i \approx 0.9$, 0.75, 0.6 and 0.4, approximately representative of buildings categorised as class A (e.g., adobe masonry), class B (e.g., simple stone masonry), class C (e.g., reinforced concrete without earthquake-resistant design) and class D (e.g., reinforced concrete with an earthquake-resistant design), respectively. Fragility curves are then generated based on the following binomial distribution

$$p_k = \frac{5!}{k!(5-k)!}\left(\frac{\mu_D}{5}\right)^k\left(1 - \frac{\mu_D}{5}\right)^{5-k} \tag{20}$$

whereby p_k is the probability of damage grade DG_k and $0 \le k \le 5$ occurring [54]. Damage grades in EMS-98 are defined as follows: no damage (DG_0), slight (DG_1), moderate (DG_2), heavy (DG_3), very heavy (DG_4) and destruction (DG_5).

Finally, fatalities are estimated by summing the effects of damage grades DG_2 to DG_5, following the HAZUS method, as indicated in Table 4 [56,57]. Fatality curves are shown in Fig. 7 for different distances d from the nearest habitation, building classes, regional attenuations and underground feedbacks, and for fixed $M_{max,tect} = 7$, volume $V = 30{,}000\,m^3$ and borehole depth $z = 6$ km. Two safety standards defined by the thresholds $IR = 10^{-6}$ and $IR = 10^{-5}$ are represented by lines in the risk space, or, in micromort units, 1 μmt and 10 μmt, respectively [58]. There are 52 fatality curves per subplot, representing the combined uncertainty on underground feedback and ground motion attenuation.

The probability p of a TLS stopping a reservoir stimulation is estimated in a frequentist manner [32], as the portion of fatality curves crossing a specified IR threshold for the case $\max(M_{max}) = M_{max,tect}$ (see Appendix C for more details on the subjective probability p and M_{max} ambiguity). Only during reservoir stimulation can the a- and b-value estimates be refined [31]. If the updated data collapsed onto a fatality curve that crosses the IR threshold, the risk-based TLS would stop the stimulation before V is reached [32]. The injection well would then be lost for the foreseeable future [10]. Thus, p also represents the probability of abandoning an injection well. Note that we assume that (a, b) is random in space, meaning that drilling close by to an abandoned well does not suggest a similar probability of failure. This may be questionable, but so far there are no data on the matter. However, underground feedback uncertainty will affect pricing via risk aversion, as demonstrated below in Section 3.4.

3.4. Behavioural decision-making model

Let us now rewrite the LCOE, or price P (see Section 3.2), as the null expectation of the following Bernoulli trial [34]:

$$(1-p)(P_{fair}E - C) + p(-C_{TLS}) = 0 = \mathbb{E}[X] = (1-p)x_1 + px_2 \tag{17}$$

with p the probability of abandoning an injection well during the stimulation phase and $C_{TLS} = C_{well} + C_{frac}$ the costs associated to the injection well loss. $X = \{x_1, x_2\}$ represents the set of possible outcomes, with x_1 a stimulation success (TLS 'green light') and x_2 a stimulation failure (TLS 'red light'). p is estimated from the seismic risk analysis set out in Section 3.3. The new LCOE is then determined as

$$P_{fair} = \frac{1}{E}\left[\left(\frac{p}{1-p}\right)C_{TLS} + C\right] \tag{18}$$

with the 'public safety cost' component represented by the TLS costs C_{TLS} weighted by the odds of the Bernoulli trial $p/(1-p)$. Note that $p = 0$ yields back $P = C/E$. The price referred to here is fair, as no risk aversion is considered despite the fact that the LCOE is now rather like a lottery.

By injecting the cost of public seismic safety into the EGS LCOE, we introduce a major source of uncertainty described by p (see Appendix C). Its impact requires an understanding of the agents' risk perception and attitude towards uncertainty, the agents here being the stakeholders of geothermal energy projects. The behavioural decision-making model adopted in this study is that of Cumulative Prospect Theory (CPT) [59], which is a generalisation of the classical Expected Utility (EUT) [60] and Subjective Expected Utility [61] theories. CPT models 'distort' interpretations of rare events, framing effects, vividness of memory, emotional effects, *etc.*, which are considered to be key factors in the context of decision-making when faced with the risks arising from induced seismicity [62].

Similarly to classical EUT, CPT determines the value of a prospect (i.e., a lottery) using an expectation operator. However, CPT differs from EUT in its definition of utility functions and probabilities. In particular, given a set of ordered consequences $X = [x_{-M} \le \cdots \le 0 \le \cdots \le x_N]$, and a probability measure $\mathbb{P} = [p_{-M}, \cdots, p_0, \cdots, p_N]$, CPT defines a value function $v(x)$, which replaces the classical utility function and depends on gain and losses, a

Table 4
Damage-fatality relationship following HAZUS MH MR3 [56].

EMS-98 grade	0	1	2	3	4	5
HAZUS grade	0	1	2	3	4-NC	4-C
Fatality rate	0	0	0.00001	0.00002	0.0002	0.1

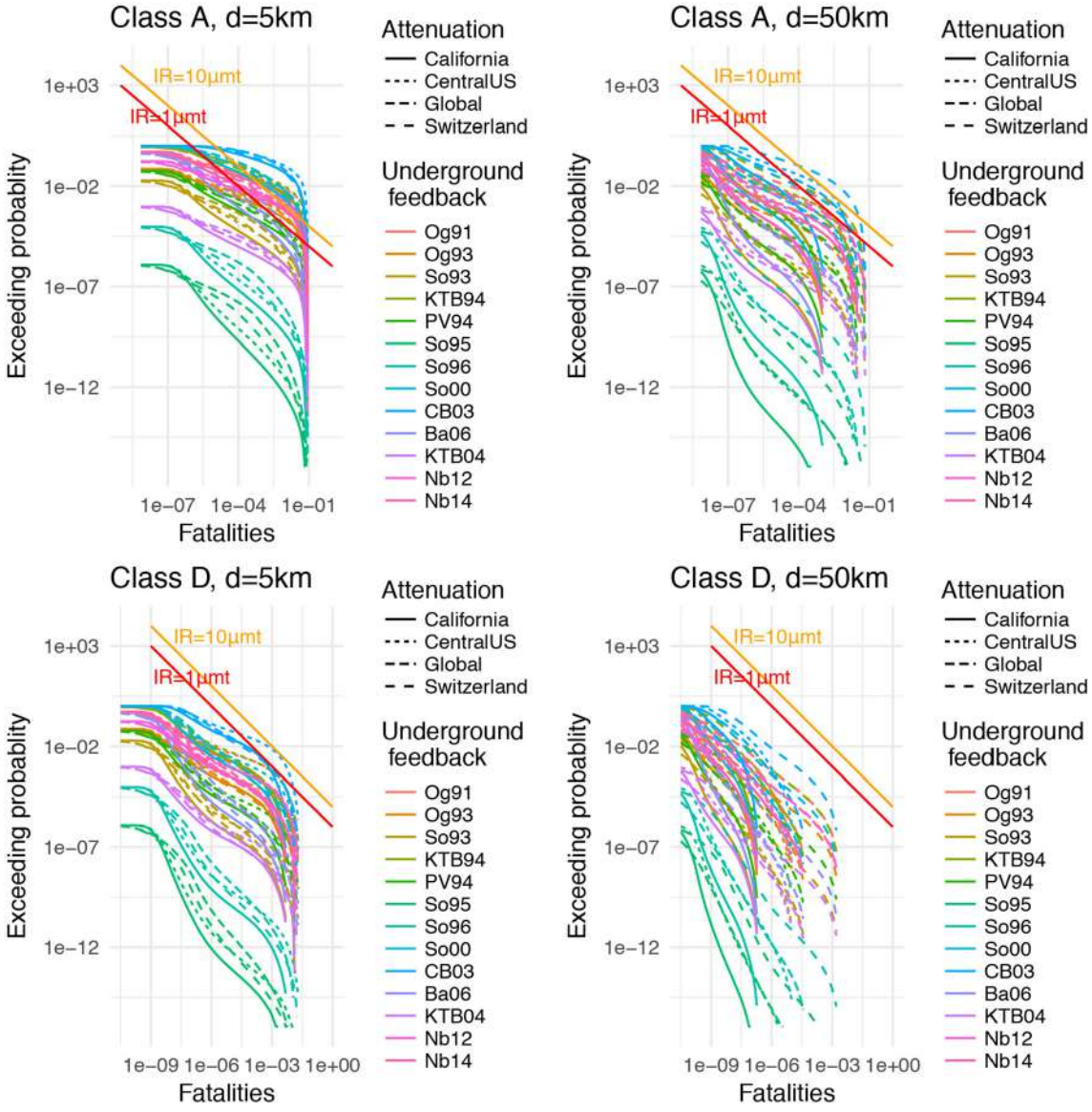

Fig. 7. Fatality risk curve scenarios for the reservoir stimulation phase, for a reservoir depth of $z = 6$ km and total injected volume $V = 30{,}000\,\mathrm{m}^3$.

loss aversion factor λ, and a weighting function $w(p)$ that maps the probability measure $\mathbb{P}$ into a 'distorted' probability measure Π. Both $v(x)$ and $w(p)$ depend on the sign of the consequences so that the functions are decomposed in $v^+(x)$ and $w^+(p)$ for positive outcomes of x, and $v^-(x)$ and $w^-(p)$ for negative outcomes. It follows that $w^-(p)$ defines the distorted probability π^-, and $w^+(p)$ defines π^+. The value $\mathscr{V}$ of a mixed prospect is then computed using the expectation operator as

$$\mathscr{V} = \mathscr{V}^+ + \mathscr{V}^- = \mathbb{E}[v(x)] = \sum_{i=0}^{N} \pi_i^+ v^+(x_i) + \sum_{i=-M}^{0} \pi_i^- v^-(x_i) \quad (19)$$

Appendix D sets out the expressions of the value and weight functions selected for the current study.

Provided Eq. (19), and given $X = [-C_{TLS}, P_{averse}E - C]$ and $\Pi = [\pi^-, \pi^+]$, we can rewrite Eq. (17) as

$$\pi^+ v^+(P_{averse}E - C) + \pi^- v^-(-C_{TLS}) = 0 = \mathbb{E}[v(x)], \quad (21)$$

or in terms of TLS-based risk-averse price,

$$P_{averse} = \frac{1}{E}\left\{(v^+)^{-1}\left[-\frac{\pi^-}{\pi^+}v^-(-C_{TLS})\right] + C\right\}, \quad (22)$$

where $(v^+)^{-1}[\cdot]$ is the inverse of $v^+(\cdot)$. Using the value and weighted functions introduced in Appendix D, we obtain

$$P_{averse} = \frac{1}{E}\left\{\left[\left(\frac{p^\delta}{(1-p)^\gamma}\frac{(p^\gamma + (1-p)^\gamma)^{1/\gamma}}{(p^\delta + (1-p)^\delta)^{1/\delta}}\right)\lambda C_{TLS}^\beta\right]^{\frac{1}{\alpha}} + C\right\}, \quad (23)$$

where $0 < \alpha \leq \beta \leq 1$ and the loss-aversion coefficient $\lambda \geq 1$ are the coefficients of the selected value function, and $0 < \gamma \leq \delta$ are the coefficients of the selected weight function. Fig. 8 shows several CPT parameterizations, as well as the mean estimate $\alpha = 0.78$, $\beta = 0.82$, $\lambda = 2.18$, $\gamma = 0.72$ and $\delta = 0.77$ that we use below (see Appendix D for a brief review of the literature).

Eq. (23) represents an important generalisation of Eq. (18), which accounts for the behaviour of the decision maker, the new pricing

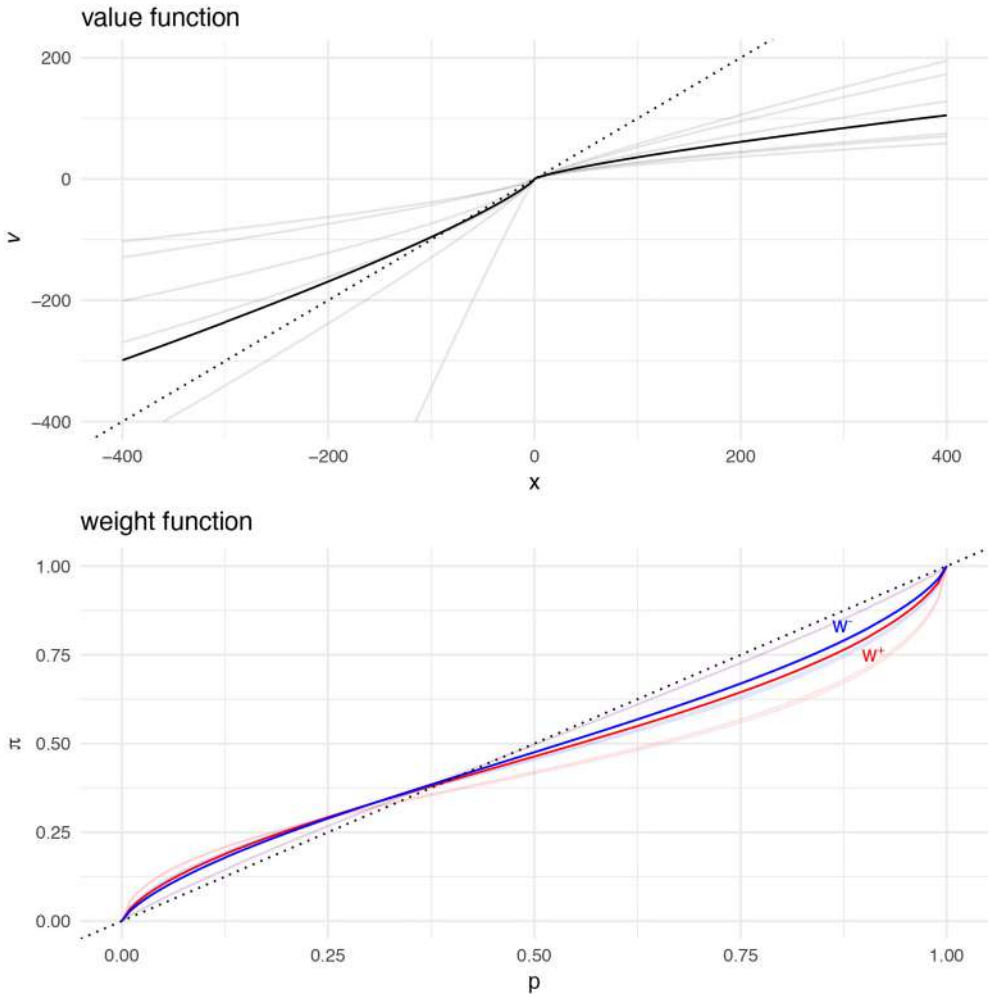

Fig. 8. CPT parameterisation for value and weight functions with mean estimates $\alpha = 0.78$, $\beta = 0.82$, $\lambda = 2.18$, $\gamma = 0.72$, and $\delta = 0.77$ (see Appendix D for different parameterisation estimates, represented here by the lighter coloured curves).

representing the decision maker's best interest in view of both risk and loss aversions. In particular, the 'public safety cost' component is represented by the *value* of the TLS costs $v^-(-C_{TLS})$ weighted by the odds of the 'distorted' Bernoulli trial π^-/π^+ composed with inverse of $v^+(\cdot)$. In other words, C_{TLS} is pushed forward to the *value* domain by the operator $v^-(\cdot)$, weighted by the 'distorted' Bernoulli trial and pulled back to the monetary domain by the inverse operator $(v^+)^{-1}(\cdot)$. If the push-forward and pull-back operators are linear, we arrive at the fair price, Eq. (18).

4. Case study

This Section presents a case study in which generic EGS triplets, as defined in Section 3.1, sell electricity and heat to a town. Section 4.1 shows the results of a sensitivity analysis of the LCOE spatial trade-off between cost of seismic risk mitigation measures and heat credit for different parameterisations; Section 4.2 illustrates the impact of different seismic safety standard values on the optimal siting of EGS plants for synthetic regions of randomly distributed towns.

4.1. Sensitivity analysis of electricity pricing subject to seismic risk/heat credit trade-off

During the stimulation phase, the plant injects a total volume $V = 30{,}000\,\mathrm{m}^3$ to create a reservoir (Section 3.1). Then the probability p of a well being lost due to an excessively high seismic risk is estimated as a function of borehole depth z and distance d, with the same underground feedback uncertainty as defined in Section 3.3 (Tables 2 and 3). Fig. 9 shows the results for different building classes and two safety standards. The probability of breaching a seismic safety standard is highest closest to the EGS plant and decreases relatively fast with an increasing distance d. The building class has a significant impact on p, with the impact felt only within 5 km of the plant for a class D building (e.g., reinforced concrete with an earthquake-resistant design) and up to tens of kilometres for a class A building (e.g., adobe masonry). Relaxing the seismic safety standard by increasing IR by one order of magnitude, from 1 μmt to 10 μmt, also significantly lowers p since the TLS is less constraining, allowing for more induced seismicity to occur during the stimulation.

Fig. 10 shows the original EGS LCOE median values P_{EGS} and P_{EGS+DH} (first row) and how the cost of TLS-based seismic risk mitigation affects P_{EGS+DH}, as a function of depth z, distance d and building class (next rows) for $IR = 10^{-6} = 1$ μmt. The impact appears negligible for the risk-neutral case while a significant reversal of the break-even price gradient over the distance d is observed for the risk-averse case, with the break-even price here fixed at 6 ¢/kWh for illustrative purposes. Because of the spatial correlation between heat credit and

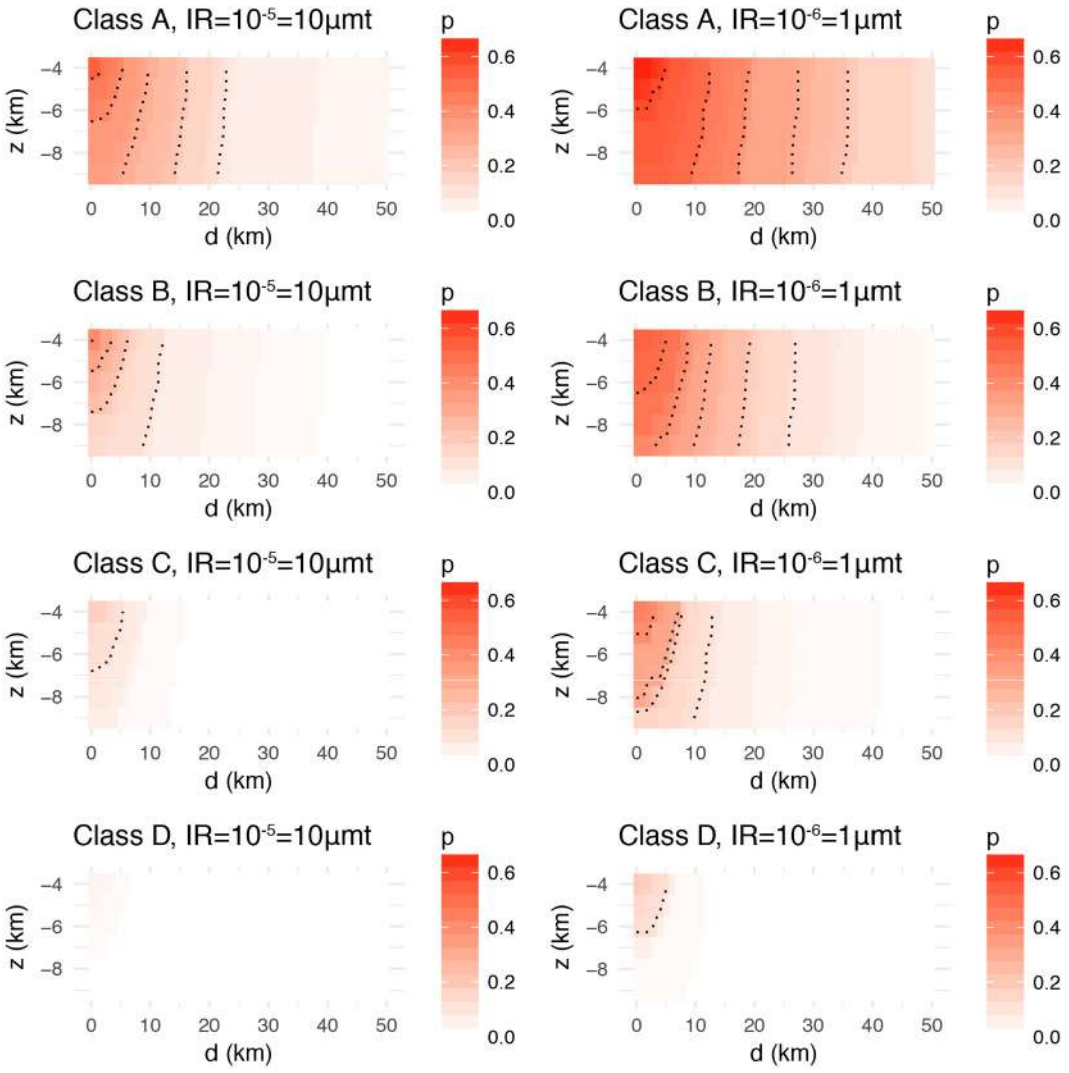

Fig. 9. Probability p of breaching a given safety standard defined by the individual risk IR.

seismic risk, an optimal distance d is observed at which the LCOE is minimal for any given depth z.

Fig. 11 shows also the original EGS LCOE median values P_{EGS} and P_{EGS+DH} (first row) and how the cost of TLS-based seismic risk mitigation affects P_{EGS+DH}, as a function of depth z, distance d and building class (next rows) for $IR = 10^{-6} = 1$ µmt, here considering the minimisation of induced seismicity during the production phase. This is done by setting the nominal flow rate $\dot{V}_{nom}$ to $\dot{V}_{cap}$ instead of $\dot{V}_{opt}$, here for $\sigma_S = 5\%$ (Fig. 3). The impact of production flow rate clipping is immediately apparent compared to Fig. 10, since the heat credit is required to break even. However, the lower plant's power exacerbates the impact of TLS risk mitigation costs on the LCOE, cancelling the heat credit for most building classes for risk- and loss-averse stakeholders. Moreover, the lower plant's power output makes district heating irrelevant at moderate to long distances, represented in grey in Fig. 11. Assuming $\sigma_S = 10\%$ [50] leads to a situation in which the break-even price is never reached and the EGS plant is likely to be terminated (not shown – all plots between purple and grey).

Our approach enables the best EGS plant site to be defined as the distance d that minimises the LCOE for a given depth z. For a CPT-rational decision-maker, the best siting distance moves from 0 km (when no seismic risk is considered) to a few kilometres for a class D building stock, to tens of kilometres for a class A building stock (Fig. 10). This shift is not altered by mitigation measures during the production phase (Fig. 11). Based on a reasonable range of input values but assuming no underground feedback spatial correlation, we find that the systematic use of a TLS would significantly affect the LCOE at small distances d for low-class building stocks (A-B). The impact remains limited for higher classes (C-D).

4.2. Optimisation of the trade-off between seismic risk mitigation cost & heat credit

We define a synthetic exposure dataset composed of $n_s = 10$ towns comprising n_b buildings of class B (e.g. simple stone masonry), following Zipf's Law $\ln(\text{rank}) = A - \ln(n_b)$ [63] with $A = 10$ and rank $= \{1, \ldots, n_s\}$. This yields a power-law distribution of town sizes ranging from $n_b = 22{,}026$ to 2203 buildings and a total number of 64,514 buildings. The towns are randomly distributed over an area measuring 100 by 200 km and buildings are distributed within each town

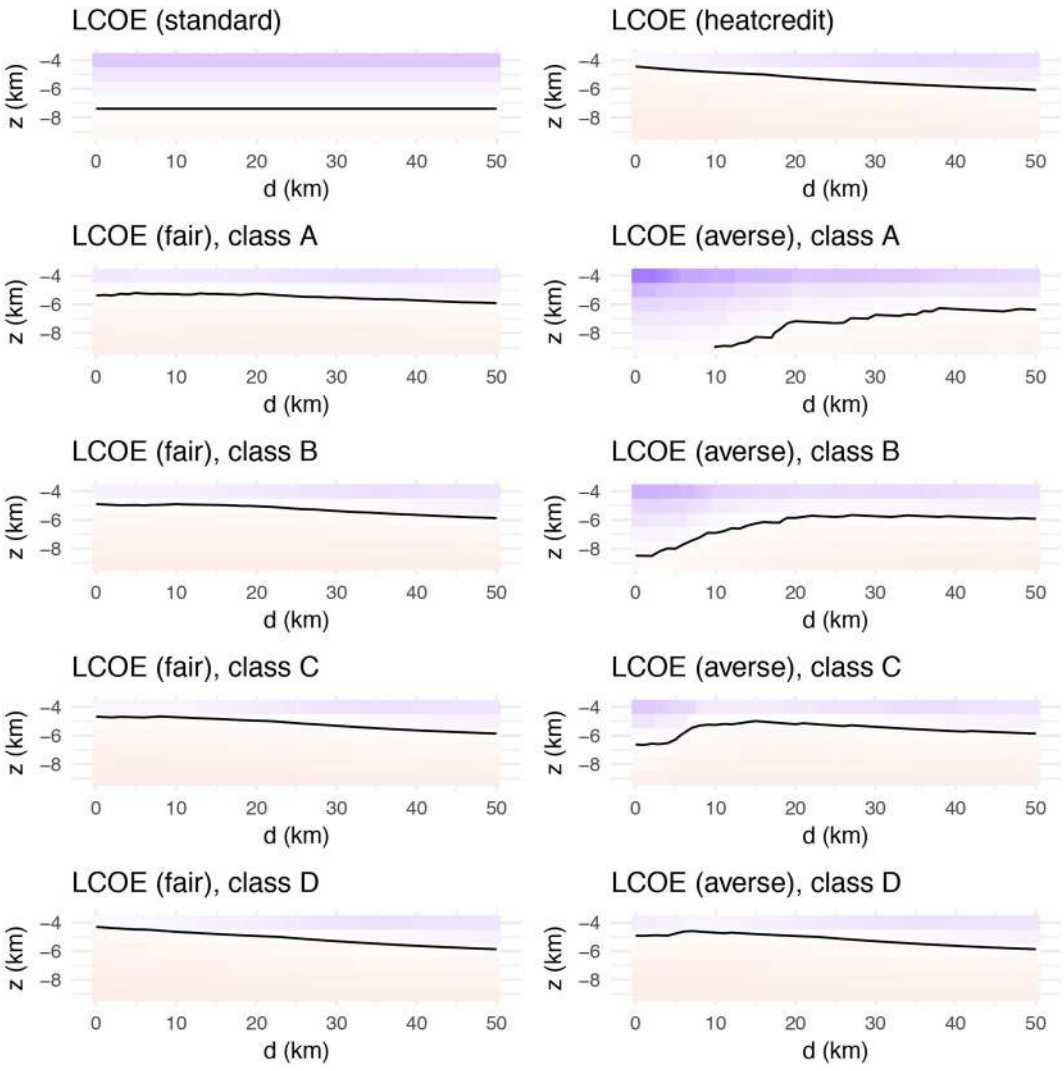

Fig. 10. Different LCOE scenarios for $\dot{V}_{nom} = \dot{V}_{opt}$ and $IR = 10^{-6} = 1$ µmt with break-even price in black, higher prices in light purple and lower prices in light red. (For interpretation of the references to colour in this figure legend, the reader is referred to the web version of this article.)

following a Brownian movement pattern, with a standard deviation of 50 m. The region needs 323 MW power bearing in mind that $\dot{E}_b = 5$ kW power per building [17]. We consider the distance d between potential EGS plants and the nearest building, assuming that there is no heat loss within a given town. For simplification, we consider that all EGS plants have a heat exchange reservoir at a depth $z = 6$ km and thus have an average power of $\dot{E}_{EGS} = 10$ MW (Figs. 2 and 5a). This yields the LCOE distance profiles and maps shown in Fig. 12, for standards $IR = 1$ µmt and 10 µmt, respectively.

In our model, siting must follow the three following rules: (1) EGS plants can only be sited in the light red regions of the maps shown in Fig. 12, which represent a competitive LCOE. This corresponds to distances in the range $19 < d < 55$ km for $IR = 1$ µmt and $0 < d < 58$ km for $IR = 10$ µmt, represented by dotted lines and curves in Fig. 12. (2) Since the LCOE(x, y) map is defined from the distance d to the nearest town, EGS plants can only distribute heat to the matching town. Each town sector is defined as a Voronoi cell and mapped in Fig. 12, along with the maximum number of EGS plants possible per sector, $n_{max} = \lceil n_b \dot{E}_b / \dot{E}_{EGS} \rceil$. (3) To meet safety standards, no given town can be prone to seismic risk from more than one EGS plant. This limit is here approximated to a circle centred at the EGS location and of radius d(min(LCOE)) c. 30 km for $IR = 1$ µmt and 13 km for $IR = 10$ µmt (see the dashed lines in the LCOE profiles).

How many EGS power plants can be built in the region? What role does the seismic safety standard threshold play in determining that number? We follow a free-market, first-come-first-served approach in which the first EGS plant is sited at a location that minimises the LCOE. Any plan to add a new EGS plant must consider the three rules set out above, whilst also trying to minimise the LCOE. Depending on the spatial distribution of towns, the resulting LCOE map and the seismic risk rule that depends on the location of existing plants, n_{max} may not always be reached. Two examples of EGS siting are shown in Fig. 13 for both safety standards, out of 50 simulated town distributions. When n_{max} is not reached for all sectors, then the total power produced by EGS plants $\dot{E}(EGS)$ is below the total 323 MW target. Fig. 13 (bottom row) shows the distribution of $\dot{E}(EGS)$ for the 50 simulated regions. We see that a stronger safety standard, here $IR = 1$ µmt compared to $IR = 10$ µmt, limits the number of possible EGS plants.

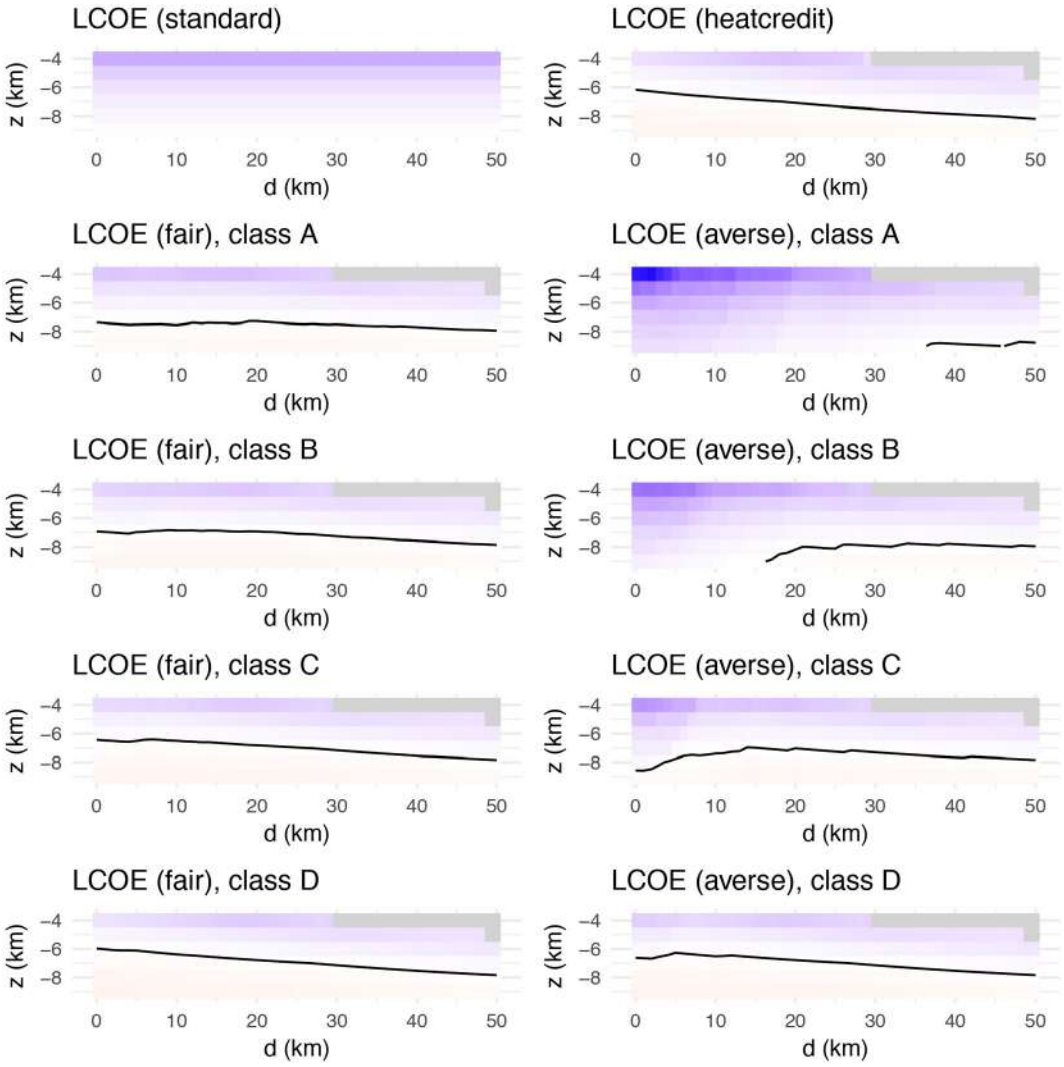

Fig. 11. Different LCOE scenarios for $\dot{V}_{nom} = \dot{V}_{cap}$ and $IR = 10^{-6} = 1$ μmt, with the break-even price in black, higher prices in light purple and lower prices in light red. (For interpretation of the references to colour in this figure legend, the reader is referred to the web version of this article.)

5. Conclusions and next directions

We have demonstrated how two different seismic risk mitigation measures could impact the EGS LCOE. Those are crucial aspects to consider in future studies on the economic viability of the EGS industry.

Projects have already been terminated due to excessively high risks during the stimulation phase, as happened in Basel in 2006 [10]. The Pohang EGS plant surely faces the same fate [48]. We have shown that siting can be optimised (i.e., LCOE can be minimised) in view of the trade-off between heat credit and seismic risk mitigation cost. Although the use of a TLS should be mandatory, we showed that the associated costs are manageable, with issues arising close to populated areas and mainly for low-class building stocks (Fig. 10). One solution includes retrofitting buildings, though this generates additional costs. We also showed that relaxing the safety standard, e.g. from $IR = 1$ μmt (micromort) to 10 μmt, would significantly lower the costs of mitigation measures because less stringent TLS thresholds would apply (Fig. 7).

We presented an example of EGS siting optimisation and illustrated the impact of different seismic safety standards on the number of possible plants (Fig. 13). Although the trade-off between protecting the public from seismic activity and safeguarding the supply of geothermal energy could be investigated within a geothermal energy risk governance framework, with the authorities, EGS firms and the general public as main stakeholders [34], selecting the *IR* standard would remain a non-trivial task, with the decision possibly based on the value of a statistical life in a given country compared to the economic potential of the EGS energy sector. However, applying economic logic to human life remains a struggle [64]. Moreover, societal aspects are an integral part of risk governance, and securing public acceptance of induced seismicity is challenging [65]. In that respect, the proposed meta-model could help to transparently communicate both costs and benefits to all actors, possibly via interactive scenarios like those illustrated in Figs. 12 and 13. Then the results could be compared by ranking different seismic safety standards against other individual and societal risks [58] or simply be used to infer the maximum percentage of the renewable energy mix that EGS could contribute for a pre-defined safety standard.

Some existing commercial EGS plants have experienced problems related to unintended induced seismicity during the production phase.

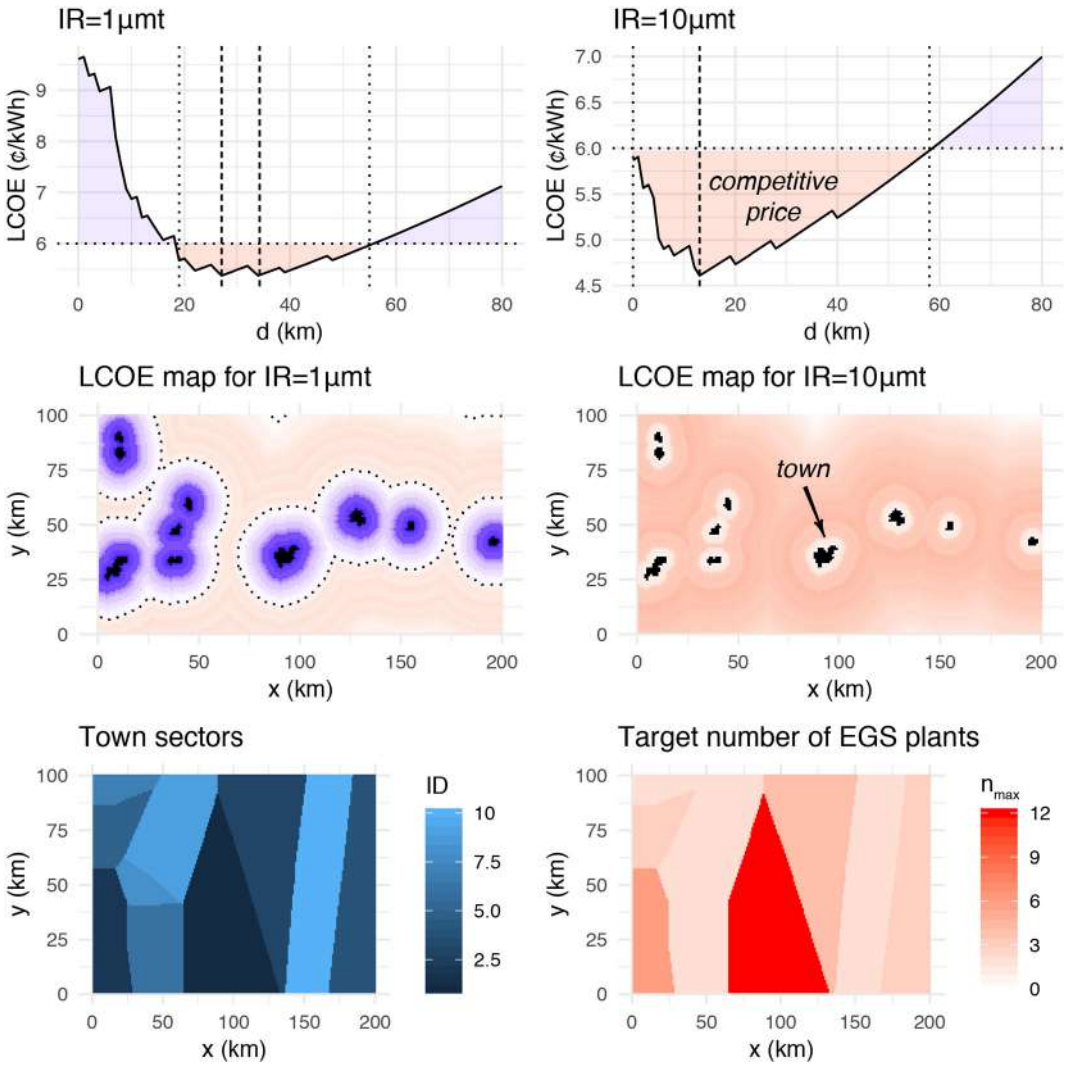

Fig. 12. Synthetic towns and associated rules for EGS plant siting.

In Soultz for instance, production flow rates were recently lowered to avoid this nuisance [9]. We showed how to predict the clipped flow rate and LCOE for a range of stress conditions (Figs. 3 and 11). We noted that the maximum overpressure at which an EGS plant can be safely operated over many years depends strongly on the stress conditions of the reservoir after the stimulation and of the plant's surroundings. Accurately predicting indicators such as σ_s, to which the estimated LCOE is sensitive, is no easy matter. However, it is clear that the lower I_{res} is, the less impact σ_s has. Consequently, EGS reservoirs that can achieve effective impedances lower than the target level for a simple doublet or triplet (e.g. multi-staged EGS) can generate just as much power while reducing potential seismicity [66]. This also highlights the need to better understand the minimum effective stress variations possible in the deep underground.

Finally, we hope that the use of algorithmic approaches will improve geothermal energy risk governance in the future. We already promoted the use of such techniques in earlier works: for safety-standard-based TLS [32], online Bayesian updating of the TLS [31], and safety-standard-based LCOE [34], in line with the actuarial approach's superiority over the clinical/expert approach [67]. As illustrated by our EGS siting optimisation case study, the issue we have taken up represents a classical artificial intelligence problem of uncertain knowledge, reasoning, and planning. To quote Russell and Norvig [68], "*decision making in the field of public policy involves high stakes, in both money and lives. For example, in deciding what levels of* [seismic shaking] *to allow from a*[n EGS] *power plant, policy makers must weigh the prevention of death and disability against the benefit of the power and the economic burden of mitigating the* [shaking]. *Siting a new* [EGS plant] *requires consideration of the disruption caused by construction, the cost of land, the distance from centres of population, the* [nuisance of EGS] *operations, safety issues arising from* [induced seismicity], *and so on*" (quote modified [between brackets] for the EGS context). With the EGS problem now formalised in terms of an LCOE optimisation problem, the meta-model could be applied to real cases, EGS siting could be improved using various optimisation approaches and renewable energy strategies could be refined.

Funding

This work was supported by the Swiss Competence Center for Energy Research – Supply of Electricity (SCCER-SoE).

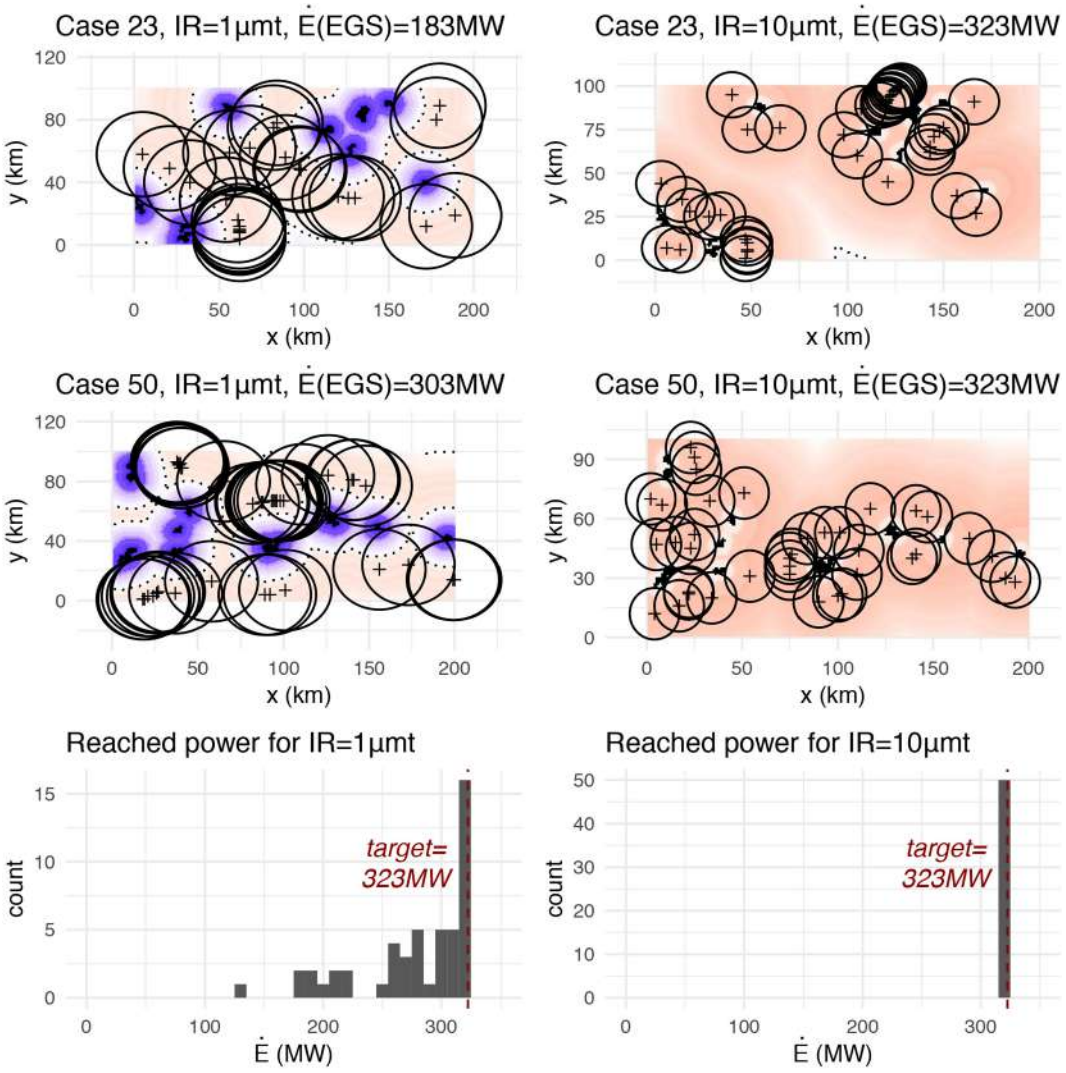

Fig. 13. EGS plant siting optimization following a free market approach.

Appendix A. EGS cylindrical well pressure loss model

A constant diameter D_w is considered for all wells' segments below a threshold depth z_0 as depicted in Fig. 1. Pressure losses per metre of depth below z_0 depth equal

$$\frac{dP}{dz} = f_D \frac{\rho}{2} \frac{u^2}{D_w} = f_D \frac{8\rho}{\pi^2 D_w^5} \dot{V}^2 \tag{A.1}$$

where u is the mean velocity of the fluid of density ρ, $\dot{V} = \pi (D_w/2)^2 u$ is the flow rate, and f_D is the Darcy friction. The empirical Blasius fit [70] yields $f_D = 0.316 \cdot Re^{-0.25}$ with the Reynolds number

$$Re = \frac{\rho D_w u}{\mu} = \frac{4\rho}{\pi \mu D_w} \dot{V} \tag{A.2}$$

where μ is the viscosity of the fluid. Substituting f_D by its fit in Eq. (A.1) leads to

$$\frac{dP}{dz} = 0.241 \frac{\rho^{0.75} \mu^{0.25}}{D_w^{4.75}} \dot{V}^{1.75} = \frac{dI_Z}{dz} \dot{V}^{1.75} \tag{A.3}$$

where I_Z is the impedance of the well's segment below z_0, which increases linearly with depth z.

We then define the total impedance I_{well} for the EGS wells, which as stated in Ohm's law for series circuits is the sum of the impedances of each well segment of constant diameter. Thus, we finally obtain

$$I_{well} = I_{w0} \left(\frac{a_{inj}}{N_{inj}^{1.75}} + \frac{1}{N_{prod}^{1.75}} \right) + (z - z_0) \left(\frac{\frac{dI_{z,inj}}{dZ}}{N_{inj}} + \frac{\frac{dI_{z,prod}}{dZ}}{N_{prod}} \right) \tag{A.4}$$

where the first term is the effective impedance above z_0, taken from the literature (the geometry of the wells above z_0 is therefore implicit), and the second term is the sum of the impedances of the injection and production segments below z_0, obtained from Eq. (A.3). a_{inj} is a factor correcting for the narrowing of the flow path in the injection well. Finally, the overall pressure losses along all wells in the EGS cycle are $\Delta P_{well} = I_{well}\dot{V}_{inj}^{1.75}$.

Appendix B. Optimal flow rate solution

Let us resolve Eq. (6), which is as follows

$$\begin{cases} f(\dot{V}_{opt}) = 2.75a\dot{V}_{opt}^{1.75} + 2b\dot{V}_{opt} + c = 0 \\ a = -I_{well} \\ b = -\frac{I_{res}}{N_{res}} \\ c = \eta_{el}\rho_{inj}c\left(T_0 + z\frac{dT}{dz} - T_{inj}\right) + zg(\rho_{inj} - \rho_{prod}) \end{cases} \tag{B.1}$$

Since it is a polynomial function with a fractional power in the first term, we resolve its Taylor expansion at $\dot{V}_0$, an initial 'guess' estimate of $\dot{V}_{opt}$,

$$f(\dot{V}_{opt}) \approx (2.75a\dot{V}_0^{1.75} + 2b\dot{V}_0 + c) + (4.8125a\dot{V}_0^{0.75} + 2b)(\dot{V}_{opt} - \dot{V}_0) + \frac{1}{2}(3.6094a\dot{V}_0^{-0.25})(\dot{V}_{opt} - \dot{V}_0)^2 = 0 \tag{B.2}$$

taking the form of this quadratic equation:

$$\begin{cases} A_1\Delta\dot{V}^2 + B_1\Delta\dot{V} + C_1 = 0 \\ A_1 = \frac{1}{2}(3.6094a\dot{V}_0^{-0.25}) \\ B_1 = 4.8125a\dot{V}_0^{0.75} + 2b \\ C_1 = 2.75a\dot{V}_0^{1.75} + 2b\dot{V}_0 + c \end{cases} \tag{B.3}$$

where $\Delta\dot{V} = \dot{V}_{opt} - \dot{V}_0$ and

$$2.75a\dot{V}_0^2 + 2b\dot{V}_0 + c = 0 \tag{B.4}$$

represents a reasonable approximate $f(\dot{V}_{opt})$ of only 2 Taylor derivatives. Resolving the two quadratic equations (B.3) and (B.4) finally yields $\dot{V}_{opt}$.

Appendix C. Subjective probability p & M_{max} ambiguity

The probability p is defined as the portion of fatality curves crossing a specified IR threshold. This assumes equal weight for all curves, following the principle of indifference [71]. Despite using all available information for seismic risk parameterisation, p is subjective, representing a so-called second-order probability in Subjective Expected Utility Theory [61]. We assumed that the (a, b) parameter scattering is representative for the parameter space, whereas this might not be the case: the distribution could be uniform and the space could extend to higher a-values. However, the assumption is reasonable, because it is restricted to a simple parameter space that can be constrained by data [72].

We only consider the case $\max(M_{max}) = M_{max,tect}$ when estimating p, because M_{max} selection is more pathological. Although M_{max} distributions are available [49], the choice of any specific weight in this context is open to debate [73]. Our initial choice was to only consider the extremes $M_{max,McGarr}(V) = 3.9$ and $M_{max,tect} = 7$ in line with decision making under ambiguity. We then adopted a 'pessimistic' minimax approach, which entails minimising potential loss in the maximum loss scenario [73–75]. Formalising the aforementioned problem with the action set $A = \{a_1, a_2\}$ with a_1 'cancel well drill' and a_2 'approve well drill' decided during project planning, and the state set $S = \{s_1, s_2\}$ with s_1 'safety criterion respected' and s_2 'safety criterion not respected', the best course of action is to choose $\min_{a\in A}[\max_{s\in S} a(s)]$. The maximum loss scenario occurs when the safety criterion is not respected, which is more likely for $\max(M_{max}) = M_{max,tect}$. Minimising the loss then involves cancelling well drilling. This is equivalent to a stress test where the extreme case (i.e., $\max(M_{max})$) is the principal scenario scrutinised. For this reason, we do not consider $M_{max,McGarr}(V)$ to evaluate p. The recent Pohang earthquake clearly shows the importance of considering $M_{max,tect}$ instead of $M_{max,McGarr}$ in risk studies (Fig. 6b). Only if the absence of pre-loaded faults in the vicinity of the EGS plant could be demonstrated could $M_{max,McGarr}$ be applied. Note, however, that external 'loading' could also stem from underground gas overpressure. Of course, one could prefer to be optimistic and use instead a maximax approach to maximise gains, disregarding potential losses [75].

Appendix D. Parameterisation of Cumulative Prospect Theory (CPT)

In CPT, a prospect is defined as a random experiment with a set of outcomes x_i and probabilities p_i. The standard notation for a prospect is (x_1, p_1, …, x_n, p_n). In this paper, we focus on a two-outcome prospect, that is ($-C_{TLS}$, p; $P_{averse}E - C$, $1 - p$). In original CPT, both the value function $v(x)$ (substituting for utility function) and the weighting function $w(p)$ (transforming the probability p_i into the distorted probabilities π_i^+ and π_i^-) depends on a wealth level, or reference point, which represents the status quo. Although this aspect can be significant, no robust mathematical models including the reference point effect have yet been fully developed [62,76]. Therefore, as following the commonly adopted approach in seismic design preference [62], the intention should be to make $v(x)$ and $w(p)$ invariant with respect to the reference point, which is fixed at 0 (the status quo before the project takes place). In CPT, the distorted probabilities π_i^+ and π_i^- are determined as the differential terms of the weighted cumulative and complementary cumulative distribution, as follows

$$\begin{cases} \pi_i^- = w^-\left(\sum_{j=-M}^{i} p_j\right) - w^-\left(\sum_{j=-M}^{i-1} p_j\right) \\ \pi_i^+ = w^+\left(\sum_{j=i}^{N} p_j\right) - w^+\left(\sum_{i+1}^{N} p_j\right) \end{cases} \tag{D.1}$$

where $w^-(0) = w^+(0) = 0$. In the proposed two-outcome mixed prospect, Eq. (D.1) reduces to

Table D1
Excerpt from Booij et al. (2010) regarding CPT parameterisation[a] in the literature.

Reference	λ	α	β	γ	δ
[59]	2.25	0.88	0.88	0.61	0.69
[80]	N/A	N/A	N/A	0.60	0.70
[81]	3.20	0.68	0.74	N/A	N/A
[82]	1.07	0.81	0.80	0.76	0.76
[78]	2.54	0.72	0.73	N/A	N/A
[83]	2.61	0.86	1.06	N/A	N/A
[84]	1.38	0.71	0.72	0.91	0.91

[a] We only considered references where values for the sets (λ, α, β) and/or (γ, δ) were provided.

$$\begin{cases} \pi_i^- = w^-(p) - w^-(0) = w^-(p) \\ \pi_i^+ = w^+(1-p) - w^+(0) = w^-(1-p) \end{cases} \tag{D.2}$$

i.e., the original prospect theory put forward by Kahneman and Tversky [77] coincides with their more recent cumulative version of 1992 [78]. The value function $v(x)$ is typically modelled by two power functions as

$$v(x) = \begin{cases} v^+(x) = x^\alpha & \text{if } x \geq 0 \\ v^-(x) = -\lambda(-x)^\beta & \text{if } x < 0 \end{cases} \tag{D.3}$$

where $0 < \alpha < \beta < 1$ are exponent parameters. The value function is concave for gains (i.e., risk averse) and convex for losses (i.e., risk seeking), with loss aversion quantified by a steeper utility function represented by the loss-aversion coefficient $\lambda > 1$. The probability weighting function of the original CPT (and adopted in this study) is formulated as follows:

$$\begin{cases} w^+(p) = \frac{p^\gamma}{(p^\gamma + (1-p)^\gamma)^{1/\gamma}} \\ w^-(p) = \frac{p^\delta}{(p^\delta + (1-p)^\delta)^{1/\delta}} \end{cases} \tag{D.4}$$

with the coefficients $\gamma < 1$ and $\delta < 1$, w^+ for gains and w^- for losses. Using Eq. (D.4) within Eq. (D.2), we obtain

$$\begin{cases} \pi_i^+ = w^+(1-p) = \frac{(1-p)^\gamma}{(p^\gamma + (1-p)^\gamma)^{1/\gamma}} \\ \pi_i^- = w^-(p) = \frac{p^\delta}{(p^\delta + (1-p)^\delta)^{1/\delta}} \end{cases} \tag{D.5}$$

and the Bernoulli 'subjective' odds as

$$\frac{\pi_i^-}{\pi_i^+} = \frac{w^-(p)}{w^+(1-p)} = \frac{p^\delta}{(1-p)^\gamma} \frac{(p^\gamma + (1-p)^\gamma)^{1/\gamma}}{(p^\delta + (1-p)^\delta)^{1/\delta}} \tag{D.6}$$

Note that the condition $\lambda = \gamma = \delta = \alpha = \beta = 1$ comes down to von Neumann and Morgenstern' original EUT with linear utility function [60]. There is a significant body of literature on the estimation of the coefficients α, β, λ, γ, and δ. Moreover, there are several formulations of the value and weight functions (see [79] for a review). Quantifying the uncertainty of parameter values and functional forms, or how these uncertainties impact the cost of energy is beyond the scope of this paper. A detailed analysis and estimation of the parameters in the context of induced seismicity would require a specific set of experiments and a separate study. In view of these considerations, we adopt $\alpha = 0.78$, $\beta = 0.82$, $\lambda = 2.18$, $\gamma = 0.72$, and $\delta = 0.77$, which are the mean estimates of several parameter estimations for the value and weight functions considered by Booij et al. [79], and reported in Table D1.

References

[1] Ellsworth WL. Injection-induced earthquakes. Science 2013;341. https://doi.org/10.1126/science.1225942.
[2] van Thienen-Visser K, Breunese JN. Induced seismicity of the Groningen gas field: history and recent developments. Lead Edge 2015;34:664–71. https://doi.org/10.1190/tle34060664.1.
[3] White JA, Foxall W. Assessing induced seismicity risk at CO_2 storage projects: recent progress and remaining challenges. Int J Greenhouse Gas Control 2016;49:413–24. https://doi.org/10.1016/j.ijggc.2016.03.021.
[4] Majer EL, Baria R, Stark M, Oates S, Bommer J, Smith B, et al. Induced seismicity associated with Enhanced Geothermal Systems. Geothermics 2007;36:185–222. https://doi.org/10.1016/j.geothermics.2007.03.003.
[5] Wittneben BBF. The impact of the Fukushima nuclear accident on European energy policy. Env Sci Pol 2012;15:1–3. https://doi.org/10.1016/j.envsci.2011.09.002.
[6] Hansen J, Kharecha P. Cost of carbon capture: can young people bear the burden? Joule 2018;2:1396–409. https://doi.org/10.1016/j.joule.2018.07.035.
[7] Grigoli F, et al. The November 2017 M_w 5.5 Pohang earthquake: a possible case of induced seismicity in South Korea. Science 2018. https://doi.org/10.1126/science.aat2010.
[8] Bommer JJ, Oates S, Cepeda JM, Lindholm C, Bird J, Torres R, et al. Control of hazard due to seismicity induced by a hot fractured rock geothermal project. Eng Geol 2006;83:287–306. https://doi.org/10.1016/j.enggeo.2005.11.002.
[9] Schill E, Genter A, Cuenot N, Kohl T. Hydraulic performance history at the Soultz EGS reservoirs from stimulation and long-term circulation tests. Geothermics 2017;70:110–24. https://doi.org/10.1016/j.geothermics.2017.06.003.
[10] Giardini D. Geothermal quake risks must be faced. Nature 2009;462:848–9.
[11] Olasolo P, Juarez MC, Olasolo J, Morales MP, Valdani D. Economic analysis of Enhanced Geothermal Systems (EGS). A review of software packages for estimating and simulating costs. Appl Therm Eng 2016;104:647–58. https://doi.org/10.1016/j.applthermaleng.2016.05.073.
[12] Lacirignola M, Blanc I. Environmental analysis of practical design options for enhanced geothermal systems (EGS) through life-cycle assessment. Renew Energy 2013;50:901–14. https://doi.org/10.1016/j.renene.2012.08.005.
[13] Bartlett S, Dujardin J, Kahl A, Kruyt B, Manson P, Lehning M. Charting the course: a possible route to a fully renewable Swiss power system. Energy 2018. https://doi.org/10.1016/j.energy.2018.08.018.
[14] Iqbal M, Azam M, Naeem M, Khwaja AS, Anpalagan A. Optimization classification, algorithms and tools for renewable energy: a review. Renew Sustain Energy Rev 2014;39:640–54. https://doi.org/10.1016/j.rser.2014.07.120.
[15] Jha S Kr, Bilalovic J, Jha A, Patel N, Zhang H. Renewable energy: present research and future scope of Artificial Intelligence. Renew Sustain Energy Rev 2017;77:297–317. https://doi.org/10.1016/j.rser.2017.04.018.
[16] Mengelkamp E, Gärttner J, Rock K, Kessler S, Orsini L, Weinhardt C. Designing microgrid energy markets A case study: the Brooklyn microgrid. Appl Energy

2018;2010:870–80. https://doi.org/10.1016/j.apenergy.2017.06.054.
[17] Noor S, Yang W, Guo M, van Dam KH, Wang X. Energy Demand Side Management within micro-grid networks enhanced by blockchain. Appl Energy 2018;228:1385–98. https://doi.org/10.1016/j.apenergy.2018.07.012.
[18] Bertani R. Geothermal power generation in the world 2010–2014 update report. Geothermics 2016;60:31–43. https://doi.org/10.1016/j.geothermics.2015.11.003.
[19] Lu S-M. A global review of enhanced geothermal system (EGS). Renew Sustain Energy Rev 2018;81:2902–21. https://doi.org/10.1016/j.rser.2017.06.097.
[20] MIT. The future of geothermal energy, impact of enhanced geothermal systems (EGS) on the United States in the 21st Century, Massachusetts Institute of Technology; 2006. ISBN: 0-615-13438-6.
[21] Tester JW, et al. Impact of enhanced geothermal systems on US energy supply in the twenty-first century. Phil Trans R Soc A 2007;365:1057–94. https://doi.org/10.1098/rsta.2006.1964.
[22] Hirschberg S, Wiemer S, Burgherr P, editors. Energy from the earth, deep geothermal as a resource for the future? Centre for Technology Assessment, TA Swiss; 2015. p. 447. https://doi.org/10.3218/3655-8.
[23] Limberger J, Calcagno P, Manzella A, Trumpy E, Boxem T, Pluymackers MPD, et al. Assessing the prospective resource base for enhanced geothermal systems in Europe. Geoth Energ Sci 2014;2:55–71. https://doi.org/10.5194/gtes-2-55-2014.
[24] Beckers KF, Lukawski MZ, Anderson BJ, Moore MC, Tester JW. Levelized costs of electricity and direct-use heat from Enhanced Geothermal Systems. J Renew Sustain Energy 2014;6:013141. https://doi.org/10.1063/1.4865575.
[25] Häring MO, Schanz U, Ladner F, Dyer BC. Characterisation of the Basel 1 enhanched geothermal system. Geothermics 2008;37:469–95. https://doi.org/10.1016/j.geothermics.2008.06.002.
[26] Knoblauch TAK, Trutnevyte E. Siting enhanced geothermal systems (EGS): heat benefits versus induced seismicity risks from an investor and societal perspective. Energy 2018. https://doi.org/10.1016/j.energy.2018.04.129.
[27] Jain C, Vogt C, Clauser C. Maximum potential for geothermal power in Germany based on engineered geothermal systems. Geotherm Energy 2015;3:15. https://doi.org/10.1186/s40517-015-0033-5.
[28] Mignan A, Landtwing D, Kästli P, Mena B, Wiemer S. Induced seismicity risk analysis of the 2006 Basel, Switzerland, Enhanced Geothermal System project: influence of uncertainties on risk mitigation. Geothermics 2015;53:133–46. https://doi.org/10.1016/j.geothermics.2014.05.007.
[29] Bosman K, Baig A, Viegas G, Urbancic T. Towards an improved understanding of induced seismicity associated with hydraulic fracturing. First Break 2016;34:61–6.
[30] Baker JW, Gupta A. Bayesian treatment of induced seismicity in probabilistic seismic-hazard analysis. Bull Seismol Soc Am 2016;106:860–70. https://doi.org/10.1785/0120150258.
[31] Broccardo M, Mignan A, Wiemer S, Stojadinovic B, Giardini D. Hierarchical Bayesian modelling of fluid-induced seismicity. Geophys Res Lett 2017;44:11357–67. https://doi.org/10.1002/2017GL075251.
[32] Mignan A, Broccardo M, Wiemer S, Giardini D. Induced seismicity closed-form traffic light system for actuarial decision-making during deep fluid injections. Sci Rep 2017;7:13607. https://doi.org/10.1038/s41598-017-13585-9.
[33] Jonkman SN, van Gelder PHAJM, Vrijling JK. An overview of quantitative risk measures for loss of life and economic damage. J Hzardous Mater 2003;A99:1–30. https://doi.org/10.1016/S0304-3894(02)00283-2.
[34] Mignan A, Broccardo M, Wiemer S, Giardini D. Autonomous decision-making against induced seismicity in deep fluid injections. Ferrari A, Laloui L (Eds.), Energy geotechnics, SEG 2018; 2019. p. 369–76. doi: 10.1007/978-3-319-99670-7_46.
[35] Zarrouk SJ, Moon H. Efficiency of geothermal power plants: a worldwide review. Geothermics 2014;51:142–53. https://doi.org/10.1016/j.geothermics.2013.11.001.
[36] Eaton BA. Fracture gradient prediction and its application in oilfield operations. J PetrolTechnol 1969;21:1353–60.
[37] Lukawski MZ, Anderson BJ, Augustine C, Capuano Jr. LE, Beckers KF, Livesay B, et al. Cost analysis of oil, gas, and geothermal well drilling. J Petrol Sci Eng 2014;118:1–14. https://doi.org/10.1016/j.petrol.2014.03.012.
[38] Persson U, Werner S. Heat distribution and the future competitiveness of district heating. Appl Energy 2011;88:568–76. https://doi.org/10.1016/j.apenergy.2010.09.020.
[39] Gerber L, Maréchal F. Environomic optimal configurations of geothermal energy conversion systems: application to the future construction of Enhanced Geothermal Systems in Switzerland. Energy 2012;45:908–23. https://doi.org/10.1016/j.energy.2012.06.068.
[40] Frick S, Kaltschmitt M, Schöder G. Life cycle assessment of geothermal binary power plants using enhanced low-temperature reservoirs. Energy 2010;35:2281–94. https://doi.org/10.1016/j.energy.2010.02.016.
[41] Broccardo M, Danciu L, Stojadinovic B, Wiemer S. Individual and societal risk metrics as parts of a risk governance framework for induced seismicity. 16th world conference on earthquake engineering; 2017.
[42] Dinske C, Shapiro SA. Seismotectonic state of reservoirs inferred from magnitude distributions of fluid-induced seismicity. J Seismol 2013;17:13–25. https://doi.org/10.1007/s10950-012-9292-9.
[43] Mignan A. Static behaviour of induced seismicity. Nonlin Process Geophys 2016;23:107–13. https://doi.org/10.5194/npg-23-107-2016.
[44] Evans KF, Zappone A, Kraft T, Deichmann N, Moia F. A survey of the induced seismic responses to fluid injection in geothermal and CO_2 reservoirs in Europe. Geothermics 2012;41:30–54. https://doi.org/10.1016/j.geothermics.2011.08.002.
[45] McGarr A. Seismic moments and volume changes. J Geophys Res 1976;81:1487–94.
[46] McGarr A. Maximum magnitude earthquakes induced by fluid injection. J Geophys Res Solid Earth 2014;119:1008–19. https://doi.org/10.1002/2013JB010597.
[47] van der Elst NJ, Page MT, Weiser DA, Goebel THW, Hosseini SM. Induced earthquake magnitudes are as large as (statistically) expected. J Geophys Res Solid Earth 2016;121:4575–90. https://doi.org/10.1002/2016JB012818.
[48] Kim K-H, et al. Assessing whether the 2017 M_w 5.4 Pohang earthquake in South Korea was an induced event. Science 2018. https://doi.org/10.1126/science.aat6081.
[49] Bommer JJ, van Elk J. Comment on “the maximum possible and the maximum expected earthquake magnitude for production-induced earthquakes at the gas field in groningen, the Netherlands” by Gert Zöller and Matthias Holschneider. Bull Seismol Soc Am 2017;107. https://doi.org/10.1785/0120170040.
[50] Gischig VS, Wiemer S. A stochastic model for induced seismicity based on non-linear pressure diffusion and irreversible permeability enhancement. Geophys J Int 2013;194:1229–49. https://doi.org/10.1093/gji/ggt164.
[51] Atkinson GM, Wald DJ. “Did You Feel It?” intensity data: a surprisingly good measure of earthquake ground motion. Seismol Res Lett 2007;78:362–8.
[52] Fäh D, Kind F, Lang K, Giardini D. Earthquake scenario for the city of Basel. Soil Dyn Earthquake Eng 2001;21:405–13.
[53] Allen TI, Wald DJ, Worden CB. Intensity attenuation for active crustal regions. J Seismol 2012;16:409–33. https://doi.org/10.1007/s10950-012-9278-7.
[54] Lagomarsino S, Giovinazzi S. Macroseismic and mechanical models for the vulnerability and damage assessment of current buildings. Bull Earthq Eng 2006;4:415–43. https://doi.org/10.1007/s10518-006-9024-z.
[55] Grünthal G, editor. European macroseismic scale, Cahiers du Centre Européen de Géodynamique et de Séismologie, 15, Luxemburg; 1998.
[56] HAZUS MH MR3. Multi-hazard loss estimation methodology: earthquake model, technical manual. Washington D.C.: NIST; 2003.
[57] Galanis P, Svcheva A, Mimra W, Stojadinovic B. A framework to evaluate the benefit of seismic upgrading. Earthquake Spectra 2018. https://doi.org/10.1193/120316EQS221M. [in press].
[58] Howard RA. On making life and death decisions. In: Schwing RC, Albers WA, Schwing RC, Albers WA, editors. Societal risk assessment, how safe is safe enough? Springer; 1980. p. 89–114.
[59] Tversky A, Kahneman D. Advances in prospect theory: cumulative representation of uncertainty. J Risk Uncertain 1992;5:297–323.
[60] von Neumann J, Morgenstern O. Theory of Games and economic behavior. Princeton University Press; 1944.
[61] Savage LJ. The foundations of statistics reconsidered. Fourth Berkeley symposium 1954:575–86.
[62] Goda K, Hong HP. Application of cumulative prospect theory: implied seismic design preference. Struct Saf 2008;30:506–16. https://doi.org/10.1016/j.strusafe.2007.09.007.
[63] Gabaix X. Zipf's law for cities: an explanation. Quaterly J Econ 1999:739–67.
[64] Hood K. The science of value: economic expertise and the valuation of human life in US federal regulatory agencies. Soc Stud Sci 2017;47:441–65. https://doi.org/10.1177/0306312717693465.
[65] van der Voort N, Vanclay F. Social impacts of earthquakes caused by gas extraction in the Province of Groningen, The Netherlands. Environ Impact Assess Rev 2015;50:1–15. https://doi.org/10.1016/j.eiar.2014.08.008.
[66] Li T, Shiozawa S, McClure MW. Thermal breakthrough calculations to optimize design of a multiple-stage Enhanced Geothermal System. Geothermics 2016;64:455–65. https://doi.org/10.1016/j.geothermics.2016.06.015.
[67] Dawes RM, Faust D, Meehl PE. Clinical versus actuarial judgment. Science 1989;243:1668–74.
[68] Russel SJ, Norvig P. Artificial intelligence, a modern approach. 3rd ed. New Jersey: Pearson Education Inc.; 2010. p. 1132.
[69] McDermott CI, Randriamanjatosoa ARL, Tenzer H, Kolditz O. Simulation of heat extraction from crystalline rocks: the influence of coupled processes on differential reservoir cooling. Geothermics 2006;35:321–44. https://doi.org/10.1016/j.geothermics.2006.05.002.
[70] Hager WH. Blasius: a life in research and education. Exp Fluids 2003;34:566–71. https://doi.org/10.1007/s00348-002-0582-9.
[71] Laplace P. Essai philosophique sur les probabilities. 3rd ed. Paris: Courcier Imprimeur; 1816.
[72] Gilboa I, Marinacci M. Ambiguity and the Bayesian paradigm. In: Arlo-Costa H. et al., editors. Readings in formal epistemology, Chapter 21; 2016. p. 385–439.
[73] Woordward RT, Bishop RC. How to decide when experts disagree: uncertainty-based choice rules in environmental policy. Land Econ 1997;73:492–507.
[74] Heal G, Millner A. Uncertainty and decision in climate change economics. Grantham Research Institute on Climate Change and the Environment, Working Paper No. 108; 2013.
[75] Kelsey D. Choice under partial uncertainty. Int Econ Rev 1993;34:297–308.
[76] Schmidt U. Reference dependence in cumulative prospect theory. J Math Psychol 2003;47:122–31. https://doi.org/10.1016/S0022-2496(02)00015-9.
[77] Kahneman D, Tversky A. Prospect theory: an analysis of decision under risk. Econometrica 1979;47:263–91.
[78] Abdellaoui M, Bleichrodt H, Paraschiv C. Loss aversion under prospect theory: a parameter-free measurement. Manage Sci 2007;53:1659–74. https://doi.org/10.1287/mnsc.1070.0711.
[79] Booij AS, van Praag BMS, van de Kuilen G. A parametric analysis of prospect theory's functionals for the general population. Theory Dec 2010;68:115–48. https://doi.org/10.1007/s11238-009-9144-4.
[80] Abdellaoui M. Parameter-free elicitation of utilities and probability weighting functions. Manage Sci 2000;46:1497–512.

[81] Tu Q. Empirical analysis of time preference and risk aversion CentER PhD Thesis, 142 Tilburg University; 2005.
[82] Andersen S, Harrison GW, Rutström EE. Dynamic choice behaviour: asset integration and natural reference points. Working paper, 06-07, Dept. Economics, College of Business Administration, Univ. Florida; 2006.
[83] Abdellaoui M, Bleichrodt H, L'Haridon O. A tractable method to measure utility and loss aversion under prospect theory. J Risk Uncertain 2008;36:245–66. https://doi.org/10.1007/s11166-008-9039-8.
[84] Harrison GW, Rutström EE. Expected utility theory and prospect theory: one wedding and a descent funeral. Exp Econ 2009;12:133–58. https://doi.org/10.1007/s10683-008-9203-7.

Glossary

CPT: Cumulative Prospect Theory
EGS: Enhanced Geothermal System
EUT: Expected Utility Theory
LCOE: Levelized Cost Of Electricity
TLS: Traffic Light System